Coordination Chemistry Reviews, 84 (1988) 1–45
Elsevier Science Publishers B.V., Amsterdam – Printed in The Netherlands

COMPARISON OF THE ELECTRONIC AND VIBRATIONAL SPECTRA OF COMPLEXES OF PROTOPORPHYRIN-IX, HEMEOCTAPEPTIDE, AND HEME PROTEINS

JOHN W. OWENS and CHARLES J. O'CONNOR
Department of Chemistry, University of New Orleans, New Orleans, Louisiana 70148 (U.S.A.)
(Received 14 November 1986)

CONTENTS

A. INTRODUCTION

(i) Molecular structure

Hemin and hemeoctapeptide have been widely used as model systems for heme proteins [1–7]. Hemin is the iron(III) complex of protoporphyrin-IX (Fig. 1). Hemin formally has a chloride ion attached at one of the axial positions; however this molecule is also commonly called hemin chloride. In this review the term "hemin" will be used in a broad sense and will be used synonymously with Fe(III)–protoporphyrin-IX. Thus compounds such as hemin bromide, and hemin iodide are actually Fe(III)–protoporphyrin-IX bromide and Fe(III)–protoporphyrin-IX iodide. Likewise, the compound, Fe(III)–protoporphyrin-IX diimidazole chloride will be represented simply as hemin diimidazole chloride.

0010-8545/88/$15.75

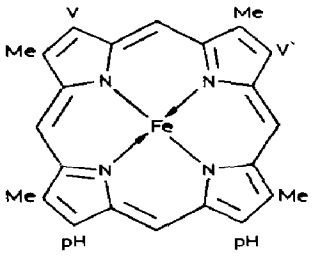

Fig. 1. Protoporphyrin-IX: Me = methyl; V = vinyl; pH = propionic acid.

Hemin is easily isolated from blood [8–10]. In actual biological systems it is the reduced ferro state which is active and binds oxygen. Protoheme is the reduced form of Fe(III)–protoporphyrin-IX and is the prosthetic group of both hemoglobin and myoglobin. Either this or a peripherally modified form is found in cytochromes and in the enzymes peroxidase and catalase [11]. Since Fe(II) is readily air oxidized to Fe(III), most investigators find it more convenient to work with ferric model systems.

The heightened interest in hemin (and its derivatives) lies in the fact that it is the active site for a variety of biochemical processes, for example oxygen bonding in hemoglobin and myoglobin. Pauling first theorized that oxygen would bind to hemoglobin only when iron was in the ferrous state [12]. This discriminating behavior is not followed by other small ligands (e.g., carbon monoxide, imidazole, nitrogen monoxide, etc.), all of which bind the iron in both the ferric and ferrous state. If the assumption is made that these other ligands are very similar to oxygen in size, charge, and bonding character, then one can use these similar ligands to infer the expected behavior of the oxygen molecule in the binding process.

The binding process for oxygen and hemoglobin has not been completely resolved. The first attempt to explain this process was presented in Perutz's theory of cooperativity [13–16]. This theory was universally accepted for several years, but was challenged in 1975 by several groups working on "cobo-globin" (complexes with hemoglobin's iron center replaced by cobalt) [17]. Perutz had claimed that (1) the binding process was controlled by the position of the metal relative to the porphyrin plane, (2) the binding of oxygen to deoxyhemoglobin caused a change in spin state, and (3) that the movement of certain amino acids was essential for the binding process to occur (e.g., for oxygen to enter the binding site) [14–16]. All of these conditions did not seem necessary for the binding of oxygen to cobo-globin complexes. More recently, Shannon's crystal structure of oxyhemoglobin [18] and Baldwin's structure of carboxyhemoglobin [19] appeared to give support to Perutz's theory, with some modifications. Hemin, met-hemoglobin and met-myoglobin ("met" indicates the ferric state of the protein)

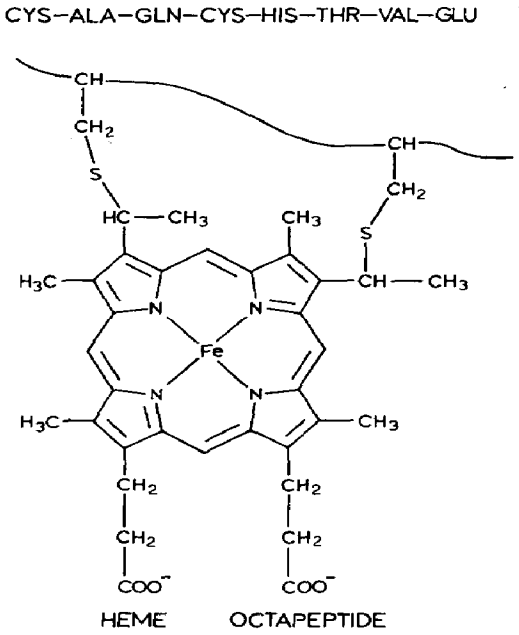

Fig. 2. Diagram of the hemeoctapeptide unit showing the peptide portion attached to the porphyrin. The histidine residue is bonded to one axial position via the imidazole group.

are usually used as substrates for the small coordinating ligands mentioned above.

Hemeoctapeptide (Fig. 2) consists of the iron porphyrin unit attached to an eight amino acid peptide chain. It was first prepared by Harbury and Loach [20] from cytochrome c, and has since been studied by several groups [21–28]. The eight amino acid chain is linked to the iron through the histidyl imidazole amino acid and to the porphyrin ring through the sulfur of the two cysteine amino acids in the small chain. Although the massive protein globin of the parent molecule is absent, the small amino acid cluster retains some of the local chemistry of the binding sites of the larger systems. Since the presence of the amino acid chain provides a more protein-like substrate for the ligands, heme-peptide complexes are likely even better models for the hemoglobin systems.

The protoporphyrin-IX macrocycle in hemin and hemeoctapeptide has a 2 − charge [29] brought about by the ionization of the two hydrogen atoms on the pyrrole nitrogen of the free acid porphyrin (pK_{a1} and pK_{a2} have been estimated at ~ 16) [30]. This charge partially satisfies the charge on the Fe(III) cation, leaving the complex with a 1 + charge. The Fe(III) accepts an electron pair from each of the pyrrolimine nitrogens as well as an electron pair from each of the negatively charged pyrrole nitrogen atoms which were formerly bonded to hydrogen. The Fe(III) protein system

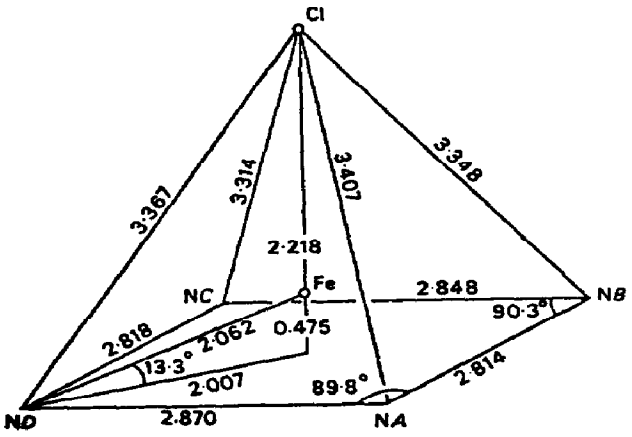

Fig. 3. Structural diagram for hemin chloride. The NA, NB, NC, and ND atoms represent the central nitrogen atoms of the porphyrin ring (taken from D.F. Koenig, Acta Crystallogr., 18 (1965) 663).

usually carries a maximum coordination number of six, and therefore either one or two ligands can coordinate. An anionic ligand can bind one of the axial positions to satisfy the 1 + charge. In Fe(III)–protoporphyrin-IX, it is the chloride ion which most frequently satisfies this charge (i.e. hemin chloride). The sixth, or remaining coordination site is left vacant. This creates an axial asymmetry in the complex, and the Fe(III) cation is displaced from the porphyrin plane and shifted toward the chloride ion (Fig. 3). Crystal structures of hemin chloride show the iron to be 0.47 Å out of the plane toward the chlorine [31].

The adjustment of charge balance by chlorine forces a local symmetry of C_{4v} on the Fe(Proto-IX)Cl coordination group, with the iron–chloride bond being coaxial with the main rotational C_4 axis. The X-ray crystal structure shows that hemin chloride assumes a square pyramidal arrangement [31].

Hemin compounds may also be axially symmetric, with identical ligands occupying the fifth and sixth coordination sites. The symmetry is then raised to D_{4h}, with a distorted octahedral arrangement (e.g. [Fe(III)(Proto-IX)$(HIm)_2$]Cl). In such highly symmetric molecules the Fe(III) ion is pulled back into the porphyrin plane.

Iron porphyrin complexes have been prepared containing a variety of ligands. These can be divided into two classes [29]: (1) five-coordinate square pyramidal and (2) six-coordinate octahedral or distorted octahedral with an axial anisotropy. When axial anisotropy is present, six-coordinate complexes of hemin may be divided into three subclasses: (i) [Fe(III)(Proto-IX)-L_2]$^+$; (ii) [Fe(III)(Proto-IX)LX]; or (iii) [Fe(III)(Proto-IX)X_2]$^-$, where

"L" and "X" represent neutral and anionic ligands respectively. Examples of subclass (iii) include $[Fe(III)(Proto\text{-}IX)(CN)_2]^-$ in pyridine solution [32,33], and in dimethyl sulfoxide (DMSO) [34]. Subclass (ii) is represented by such complexes as [Fe(III)(Proto-IX)NO(1-MeIm)] [35] and [Fe(III)(Proto-IX)HIm(CN)] [36]. Subclass (i) includes $[Fe(III)(Proto\text{-}IX)(HIm)_2]^+$ [37] and $[Fe(III)(Proto\text{-}IX)(Pyr)_2]^+$ [38]. Only one subclass of square pyramidal complexes of hemin has been reported: Fe(III)(Proto-IX)X, where $X^- = Cl^-$, Br^-, I^-, SCN^-, OAc^-, and other ions [38,39]. Only one class of ferric hemeoctapeptide has been reported: Fe(III)(H8PT)X, where $X = N_3^-$, CN^-, F^-, Im^-, etc. [21–23].

(ii) Electronic structure

The presence of ligands at axial positions tends to modulate the electronic and magnetic properties of the iron center. The Fe(III) ion is a d^5 system, and may exist in one of four possible spin states [40]: pure sextet, $^6A_1$ (high spin, $S = 5/2$); pure doublet, $^2T_2$ (low spin, $S = 1/2$); pure quartet, $^4T_1$ (intermediate spin, $S = 3/2$); or a spin-mixed state (e.g. $S = 5/2$, $S = 3/2$). Figure 4 and Table 1 show how the single d-orbital energies for the d^5 free ion configuration are perturbed by the crystal field created by the porphyrinato macrocycle and the axial ligands; it also shows how the resulting orbitals are split by the descent in symmetry from octahedral to tetragonal to rhombic ($O_h \rightarrow D_{4h} \rightarrow D_4$). The electronic configurations for the $S = 1/2$, $S = 3/2$ and $S = 5/2$ states are also shown in Fig. 5.

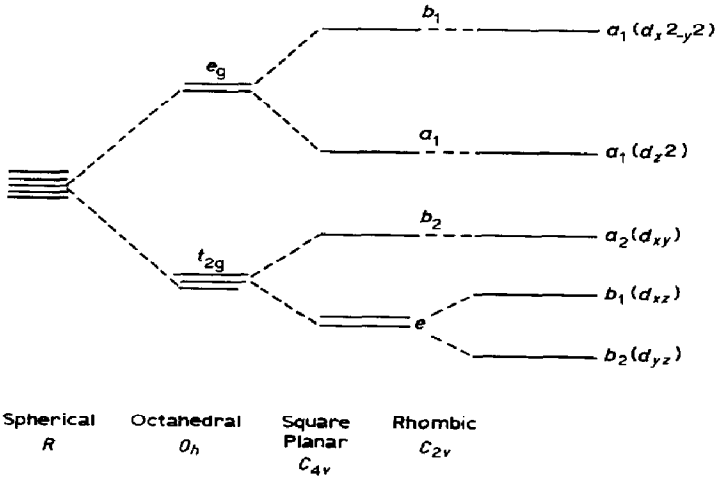

Fig. 4. Diagram showing how the $3d$ electrons are split under the influence of changes in molecular symmetry.

TABLE 1

Correlation table for the heme molecular orbitals

Conventional designation	D_{4h}	C_{4v}	C_{2v}	C_s
Porphyrin (π^*)	$b_{1u}(b_{2u})$	$b_2(b_1)$	$a_2(a_1)$	$a''(a')$
Porphyrin (π^*)	e_g	e	$b_1 + b_2$	$a'' + a'$
Iron ($d_{x^2-y^2}$)	$b_{1g}(b_{2g})$	$b_1(b_2)$	$a_1(a_2)$	$a'(a'')$
Iron (d_{z^2})	a_{1g}	a_1	a_1	a'
Iron (d_{xy})	$b_{2g}(b_{1g})$	$b_2(b_1)$	$a_2(a_1)$	$a''(a')$
Iron ($d_{xz} = d_{yz} = d$)	e_g	e	$b_1 + b_2$	$a' + a''$
Porphyrin (π)	a_{1u}	a_2	a_2	a''
Porphyrin (π)	a_{2u}	a_1	a_1	a'
Porphyrin (π)	e_g	e	$b_1 + b_2$	$a' + a''$
Porphyrin (π)	$b_{2u}(b_{1u})$	$b_1(b_2)$	$a_1(a_2)$	$a'(a'')$
Porphyrin (π)	e_u	e	$b_1 + b_2$	$a' + a''$

Many 5-coordinate ferric porphyrins are known with an assortment of axial ligands: N_3^-, F^-, Cl^- [41], OCH_3^- [42], OCl^-, CN^- [43], etc. All are high spin ($S = 5/2$), except the CN^- complex which is low spin ($S = 1/2$) [44]. For the high spin complexes, the iron atom is shifted out of the porphyrin plane toward the ligand. In low spin 5-coordinate species, the ferric atom is located closer to the porphyrin plane.

Generally, low spin ligands create strong crystal fields and provide better overlap with the metal orbitals via strong σ interaction and/or π-acceptor ability. The net result is an increased bond order and ultimately shorter iron–ligand bond lengths. The synergic effects of strong field ligands (e.g.,

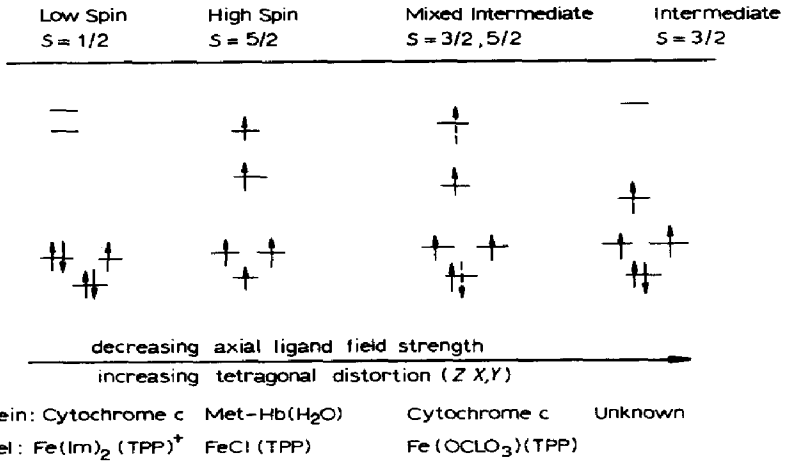

Fig. 5. $3d^5$ splitting patterns for different spin states, with representative examples for protein and model systems (taken from ref. 45).

CN^-, CO, NO, etc.) lessen the electron density on the ferric metal ion, shrinking the *d* orbital spatial radial expansion, and so the iron atom is better able to fit into the center of the porphyrin ring.

High spin ligands are often π-donors as well as σ-donors and in many cases lengthen the metal–ligand bond, as the *d* orbital π set, t_{2g} (d_{xy}, d_{xz}, d_{yz}) is raised in energy. Such high spin ligands are unable to shrink electron density about the iron core, and the *d* orbitals remain stretched in direct accordance with the lower bond order, the subsequent longer metal–ligand bond, and the displacement of the large electron rich iron away from the porphyrin plane.

Intermediate spin and quantum mixed spin states are usually found in porphinatoiron(III) complexes only when the ligand is very weak, (e.g., large radius anions, ClO_4^-, BF_4^-, PF_6^- and $CF_3SO_3^-$) [40,45]. These complexes are prepared by metathesis of the porphyrin halide with the silver salt of the appropriate large anion. Some of these systems have been characterized as thermal spin equilibrium in solution ($S = 3/2$, $S = 5/2$), but in the solid state a spin admixed state results ($S = 3/2 \leftrightarrow S = 5/2$). A true intermediate spin state ($S = 3/2$) and a spin admixed state ($S = 3/2 \leftrightarrow 5/2$) would be expected to exhibit the same species over a variable temperature range whereas a thermal spin equilibrium would exhibit two different species over the same range.

Reed and coworkers [45] explain the existence of some of these unusual hemeperchlorate complexes in terms of an axial/equatorial ligand cooperation. Since the metal–perchlorate bond must necessarily be lengthened, due to the weak field nature of the ligand (e.g. it is a good π-donor and a weak σ-donor) there is an axial elongation along the *z*-axis. The porphyrin ring contracts radially about the iron center. The contraction is consistent with depopulation of the $d_{x^2-y^2}$ orbital. The crystal field anisotropy (x, $y \gg z$) causes the $d_{x^2-y^2}$ orbital to split further apart from the nonbonding d_{xy} orbital and is raised higher in energy than the other *d* orbitals [45]. The $d_{x^2-y^2}$ orbital is then restored to an antibonding state. The overall effect is the creation of an $S = 3/2$ state (Fig. 5).

The importance of these complexes lies in the fact that it was previously believed that intermediate spin states were caused by ligands of intermediate field strength. Jorgensen's "*f*-values" place ClO_4^- alongside Cl^- and Br^- in terms of ligand field strength [46,47], but Reed labels it as a much weaker ligand than any of the halogens. This discovery of an intermediate spin state with axial metal–ligand bond lengths greater than those for metal–ligand systems of weak field strength has greatly increased our understanding of these systems.

Six-coordinate porphyrinatoiron(III) complexes exhibit all types of spin states. Low spin complexes ($S = 1/2$) are realized with ligands such as CN^-,

CO, NO, Im^-, etc. Their existence is made possible by good σ-donors and/or good π-acceptor. The iron is always in or very close to the porphinato plane in low spin complexes regardless of whether the ligands occupying the fifth and sixth axial positions are identical. Complexes such as [Fe(Proto-IX)(1-MeIm)$_2$]$^+$ [48] and [Fe(Proto-IX)(CN)$_2$]$^-$ [36] are low spin because of the reasons mentioned earlier, but it seems to be a unique property of porphyrins that the presence of one good π-acceptor fixes a low spin state for the complex regardless of the nature of the *trans* axial ligand.

(iii) Ligand coordination chemistry

Complexes with mixed axial ligands, for example [Fe(III)(Proto-IX)(LL')] (charge on complex = 1 −, 1 +, or 0), are more numerous than complexes of the type [Fe(III)(Proto-IX)L_2]$^+$ or [Fe(III)(Proto-IX)X_2]$^-$ because the binding of the first ligand exerts a *trans* labilizing effect on the binding of the second ligand of the same type [49,50]. If the crystal fields are too strong, as in CO, NO or O_2, the presence of one axially bonded ligand will prevent the binding of another of the same type. There are no known compounds of hemin which contain two carbonyl units or two nitrosyl units. Presumably, the attachment of one very strong retrobonding ligand satisfies the electronegative and electropositive nature of the iron metal, making it less likely to bond another strong field ligand.

Moderately strong field ligands such as CN^- or imidazole and their derivatives do not exert as strong a *trans* effect as the stronger π-acceptors such as carbonyls. It is this diminished π-acid ability in the former complexes that allows the formation of bis-nitrogenous porphyrinato Fe(III) complexes, while bis-carbonyl and bis-nitrosyl complexes do not exist [50]. That dicyano hemins exist and bis-carbonyls do not must be attributed to a larger σ-donor/π-acceptor ability and to the larger basicity of the cyanide, as well as its ability to neutralize effectively the charge on the iron. Nevertheless, it is clearly the large difference in *trans* effects that allow for the existence of the mixed ligand CO/pyridine hemin complexes [51] (pyridine exerting the smaller *trans* effect), while the lack of difference in *trans* effects for strong π-acceptors prohibits the formation of bis-carbonyl hemins. Even in the bis-imidazole hemins the two axial Fe–N(Im) bond distances are not equal [48]. The planes of the two imidazole rings are oriented at 90° to each other and utilize different metal *d* orbitals for π-bonding. This stereochemistry has been attributed to steric effects, but a small *trans* effect may also contribute.

The Fe–CN bond distances in the dicyano hemins are abnormally long, about 1.975 Å [52], whereas in most mono-cyano hemins, the Fe–CN bond distance is approximately 1.908 Å [53]. This increase in bond distance for

the dicyano species is also due to a diminished π-bonding between the metal and the cyanide.

There are proportionately fewer examples of six coordinate high spin species of hemin. Hemin chloride is high spin in pyridine, but there is a question of whether the pyridine actually coordinates. Hemin chloride has been characterized as five coordinate in other solvents such as benzene, chloroform, and methylene chloride [54]. In DMSO, the chlorine is displaced and two DMSO molecules occupy the axial sites [55,56]. The ligand dissociation process is faster when chloride is replaced by iodide [56]. Both $[Fe(III)Proto\text{-}IX\text{-}(DMSO)_2]^+$ and $[Fe(III)Proto\text{-}IX\text{-}(DMF)_2]^+$ have been characterized as high spin [56]. Six coordinate high spin manganese protoporphyrin species containing mixed ligands (LL′) have been characterized with L = F, Cl, Br, I, N_3, OCN, NCS and L′ = H_2O [57].

There are few reports of six coordinate hemin complexes containing symmetrical high spin ligands other than solvents. For example $[Fe(III)(Proto\text{-}IX)(N_3^-)_2]^-$ has never been reported in either the liquid or solid state. The complexes $[Fe(III)(Proto\text{-}IX)X_2]^+$, with $X = Cl^-$, I^-, Br^-, etc., simply do not exist, but the difluoro hemin complex has been reported [58]. The difluoro tetraphenyl complex has been characterized crystallographically [59]. The unique existence of the difluoro hemin must be attributed to the greater basicity and the smaller charge/radius ratio. Pearson's hard-soft acid/base theory (HSAB) [60–62] depicts fluorine as a hard base, and is easily the most compatible of the halogens with the Fe(III) metal moiety.

Buchler [29] has estimated that the effective ionic radius for low spin Fe(III) is 55 pm while that for high spin Fe(III) is 64 pm in stable ferric metalloporphyrins. The smaller size of the low spin species is attributed to backbonding [29]. This shrinking of the porphyrin ring is known as ruffling [5,63,64]. Since the 1 + charge on the hemin complex is neutralized by the first of these high spin ligands to coordinate, there is no labilization of the *trans* axial site and a second ligand does not coordinate.

The porphyrin ring is also capable of accepting π-density from the metal [5]. Its ability to drain electron density from the metal is modulated by the presence of ring substituents like vinyl groups and propionic acid side chains (Fig. 1). Electronegative substituents decrease ring basicity [65], and the overall effect is that the Fe(III) core becomes more electronegative toward the axial ligand(s). This often results in the Fe atom being displaced from the plane of the porphyrin ring in mono-ligated hemins.

The most piercing evidence of this electronegative effect is found in crystallographic X-ray determinations where it is seen that the nitrogens of the porphyrin ring actually follow the displaced iron out of the porphyrin plane. This process is known as "doming" [63,64]. The squeezing action of

the porphyrin core, the subsequent displacement of the iron out of the porphyrin plane, and the inability of the single ligand to enhance the coordination at the *trans* position tend to stabilize the five coordinate species.

Six coordinate high spin species have the metal located directly in the plane of the porphyrin ring. Such species are made possible because the porphyrin ring expands radially to admit the large iron nucleus [63,64]. For example, two tetraphenylporphyrin complexes have been isolated and characterized by X-ray crystallography: $[Fe(III)(TPP)(H_2O)_2]^+$ (TPP = tetraphenyl porphyrin) [66] and $[Fe(III)(TPP)(TMSO)_2]^+$ (TMSO = tetramethyl sulfoxide) [65]. None have been isolated for hemin derivatives. The large radial expansion of the porphyrin ring in these complexes is attributed to the population of the $d_{x^2-y^2}$ orbital [67]. The DMSO complexes such as $[Fe(III)(Proto\text{-}IX)(DMSO)_2]^+$ can exist only in solution. Whether DMSO is indeed a unique ligand with an extraordinary chemistry with hemin (e.g. allowing for 6 coordination), or whether its polarity and solvolysis make it axially more desirable than other high spin ligands (e.g., the halogens) is not known. To date there is no evidence that six coordinate high spin protoporphyrin-IX complexes with identical ligands are either thermodynamically or kinetically stable in the solid state.

B. ELECTRONIC SPECTROSCOPY

(i) Electronic transitions

The first thorough characterization of all the electronic transitions of ferric porphyrins was performed by Williams and coworkers [68,69] for several complexes of met-hemoglobin, protoporphyrin-IX, and cytochrome c. A careful analysis of the data for these complexes revealed that the positions of the bands could distinguish certain properties such as spin state, the nature of the axial ligands, and the nature of certain substituents on the porphyrin ring. Walker [37] and Kobayashi [70] have reported detailed electronic spectra for tetraphenylporphyrin complexes of imidazole and pyridine. Caughey [71] has presented a table of electronic transitions for several deutero-porphyrin complexes. Buchler has also presented a thorough review of the electronic spectra of all porphyrin types [29,49]. Later, Gouterman became influential in the assignment of these transitions [40,72–74], based largely on a theoretical extended Hückel treatment. Polarized single crystal absorption has recently been employed to characterize further the previously anomalous charge transfer transitions [75,76].

This section seeks to compare the electronic characterization of certain hemeoctapeptide and protoporphyrin complexes with those of hemoglobin.

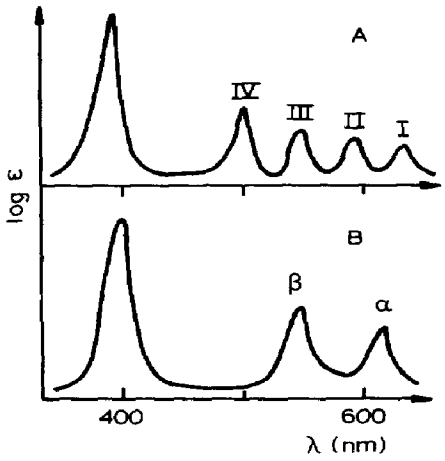

Fig. 6. (A) The Soret band (near 400 nm) and the weaker α, β bands, occurring in the visible region, for non-metallated porphyrins. (B) The same spectra as in (A), except for a metallated porphyrin.

The similarity in the positions of those bands for the model complexes (protoporphyrin-IX and hemeoctapeptide) and the native proteins are also discussed and interpreted in terms of their ability to model the protein. Our comparisons are limited to the range 200–800 nm.

A demetallated porphyrin ring contains four bands in the visible region and one band in the ultraviolet (Fig. 6). The band occurring in the ultraviolet region is called the Soret band. The four bands occurring in the visible are allowed by D_{2h} symmetry [72]. When a metal is added, the symmetry is raised to D_{4h} as two of the inner pyrrole hydrogens are replaced. This reduces the number of visible bands from four to two [72]. The positions of these two bands are dependent on metal spin state, ligand basicity, and metal oxidation state [68,69,72,73].

The Soret band, also known as the B band, occurs near 400 nm for all metallated protoporphyrin-IX and hemeoctapeptide complexes. This band also has a shoulder about 20 nm to the high energy side known as $B(1, 0)$ [76] which is due to the vibronic/electronic coupling of the porphyrin B band and the a_{1g} vibration. The two bands in the visible are called α (known as Q_0) and beta (also known as Q_v) bands. Low spin ferric porphyrins exhibit α and β bands at approximately 575 and 540 nm, respectively. However, high spin ferric porphyrins exhibit these same bands near 545 and 505 nm. The shift of the Q bands for low spin porphyrins has been attributed to displacement of the iron from the plane of the porphyrin ring [153,154]. This displacement causes a rhombic perturbation of the heme plane shifting the energy of the porphyrin $e_g(\pi^*)$ orbitals and removing the

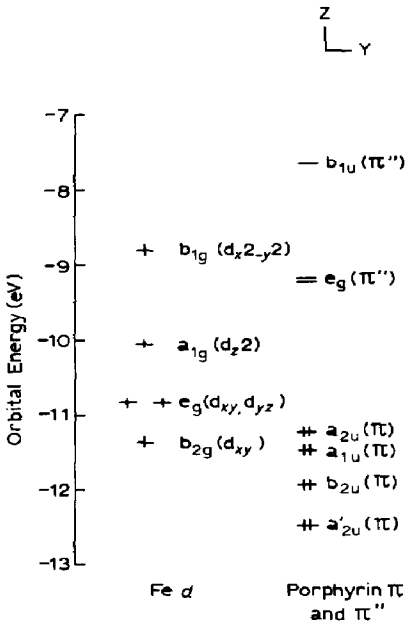

Fig. 7. The molecular orbital diagram for a typical protein complex. The metal is in a high spin state. The porphyrin orbitals are for methemoglobin (taken from A.B.P. Lever and H. Gray (Eds.), Iron Porphyrins, Elsevier, New York, 1983).

degeneracy of these orbitals. Alternatively, Gouterman [73] and coworkers have suggested that the increased crystal field splitting of the ferric d orbitals (e.g. the $t_{2g} - e_g$ separation in low spin porphyrins) has the effect of raising the energy of the a_{1u} and a_{2u} porphyrin orbitals, thus accounting for the red shift. Eaton and Hockstrasser [154] suggested configuration interaction as the primary cause of the red shift of the B and Q bands. The Soret and α-β bands all derive from the porphyrin ring π to π^* transitions (see the molecular orbital description of the π-orbitals of the porphyrin ring in Fig. 7). The possible transitions are $a_{2u} \rightarrow e_g^*$ and $a_{1u} \rightarrow e_g^*$. According to Gouterman's four-orbital model, these two transitions which transform as E_u under D_{4h} symmetry are nearly degenerate. Configuration interaction mixes these two transitions, creating a high and low energy pair [69]. The high energy Soret band is a relatively pure $\pi \rightarrow \pi^*$ electronic transition, but the low energy band (α-β, also known as the Q band) is coupled to a vibration which mixes the B and Q states [154,72,73]. The β-band, highest in energy, has been designated the $Q(1, 0)$, or Q_v, while the α-band has been assigned to the $Q(0, 0)$, or Q_0, component of a vibrational progression. In the demetallated porphyrins, the $Q(0, 0)$ band becomes split into $Q_x(0, 0)$ and $Q_y(0, 0)$, with each of these bands having overtone bands, $Q_x(1, 0)$ and $Q_y(1, 0)$ [72].

The intensity of the Soret band is normally ten times that of the α-β bands. The addition of the transition dipoles for the π–π^* transition is responsible for the intensity of the Soret band while the subtraction of the dipoles results in a low intensity for α-β bands [73].

The HOMO (highest occupied molecular orbital) is characterized by $l_z = \pm 4$, and the LUMO as $l_z = \pm 5$. Two transitions become possible ($\pm 4 \rightarrow \pm 5$) giving two pairs of excited states with total angular momentum $\langle L_z = \pm 1 \rangle$ and $\langle L_z = \pm 9 \rangle$. The ground state is $\langle L_z = 0 \rangle$, since all orbitals are filled. The two transitions become $\langle L_z = 0 \rangle \rightarrow \langle L_z = \pm 1 \rangle$ and $\langle L_z = 0 \rangle \rightarrow \langle L_z = \pm 9 \rangle$. The selection rule $L = \pm 1$ means that the ($0 \rightarrow \pm 9$) transition is not allowed. Consequently, the Soret band is observed as ($0 \rightarrow \pm 1$), and the weaker four bands located in the visible are associated with the formally forbidden ($0 \rightarrow \pm 9$) transition, which may become enabled due to configuration interaction and other effects [74].

Proof of this assignment lies in the MCD observation that the intensity times the angular momentum is exactly equal for transitions in both the Soret and visible regions [74]. The Soret band is approximately 10 times as intense as the visible bands and is associated with the $0 \rightarrow \pm 1$ transition while the low intensity visible bands are associated with the $0 \rightarrow \pm 9$ transition. This confirms the 1 : 10 ratio for the angular momentum.

A charge transfer band occurs with excitation of an electron from one atom or group of atoms to another different atom or group of atoms. With no other influences present, these charge transfer bands appear weak since the molecular orbitals are located in different regions of the complex [70,73]. In ferric metalloporphyrins, this occurs as a direct result of porphyrin $\rightarrow$ iron electron transfer. The iron $\rightarrow$ porphyrin charge transfer bands have not been definitely assigned for ferric porphyrins but have been assigned for ferrous porphyrins [76,153].

(ii) General spectroscopic features

Polarized absorption measurements [153,154] have greatly enhanced our understanding of the charge transfer (CT) bands. In general most ferrous porphyrins exhibit Fe(d) $\rightarrow$ porphyrin (π^*) CT bands for high spin complexes, with porphyrin (π) $\rightarrow$ Fe(d_{z^2}) CT transitions for corresponding low spin complexes. Ferric porphyrins generally exhibit porphyrin (π) $\rightarrow$ Fe(d) CT bands, regardless of spin state. In addition, Eaton [151] has shown that there are considerable contributions from the Fe d electron orbital splittings to the energies of all charge transfer transitions of high spin porphyrin.

The high spin ferric aquo complex of met-myoglobin [76,154] exhibits primary CT bands near 467 nm ($a_{2u'} \rightarrow d_{z^2}$), 580 nm ($a_{1u} \rightarrow d\pi$), 666 nm ($a_{2u} \rightarrow d_{z^2}$), 633 nm ($a_{2u} \rightarrow d\pi$) and 1010 nm (configurational mixing of

TABLE 2

Polarized single-crystal electronic absorption spectral data for some hemoproteins (nm) [a]

	N	B	$B(1,0)$	Q_0	$Q_v(1,0)$	$Q(3,0)$	CT bands
Ferrous							
MbCO	345	422	400	576	541	489	
low spin							645 Fe $e_g(d\pi) \rightarrow e_g(\pi^*)$
							482 Im N$(p_z) \rightarrow e_g(\pi^*)$
							286–333 $a_{2u} \rightarrow d_{z^2}$
							and $d_{xy} \rightarrow d_{x^2-y^2}$
MbO_2	348	418	398	580	542	476	645 Fe $e_g(d\pi) \rightarrow (\pi^*)$
low spin							476 $a_{2u} \rightarrow d_{z^2}$
							323 $a_{2u'} \rightarrow d_{z^2}$
							926 a_{2u}, $a_{1u} \rightarrow O_2(\pi g)$
$MbCN_2$	–	–	–	–	–	–	645 Fe $e_g(d\pi) \rightarrow e_g(\pi^*)$
low spin							476 $a_{2u} \rightarrow d_{z^2}$
							313 $a_{2u'}$, $b_{2u} \rightarrow d_{z^2}$
Deoxy Mb	–	433	406	607	–	476	627 $d_{z^2} \rightarrow e_g(\pi^*)$
high spin							685 $d_{x^2-y^2} \rightarrow e_g(\pi^*)$
							758
							816 $d\pi \rightarrow \pi^*$
							930
Ferric							
Met–Mb_2O	357	408	386	545	505		467 $a_{2u'} \rightarrow d_{z^2}$
							580 $a_{1u} \rightarrow d\pi$
high spin							666 $a_{2u} \rightarrow d_{z^2}$
							633 $a_{2u} \rightarrow d\pi$
							1010 conf. mixing
							of $^{1,2}Q_0$ and
							a_{2u}, $a_{1u} \rightarrow d\pi$
Met(CN)Mb	350	421	400	575	540		340 $a_{2u'}b_{2u} \rightarrow$
							d_{z^2}, $d_{x^2-y^2}$
							488 $a_{2u} \rightarrow d_{z^2}$
							1300 a_{2u}, $a_{1u} \rightarrow d\pi$
							800 $e_g(\pi) \rightarrow d\pi$
Met(N_3)Mb	350	420	400	575	540		340 $a_{2u'}$, $b_{2u} \rightarrow$
							d_{z^2}, $d_{x^2-y^2}$
high/low spin							488 $a_{2u} \rightarrow d_{z^2}$
						hs	625 a_{2u}, $a_{1u} \rightarrow d\pi$
						ls	690 $e_g(\pi) \rightarrow d\pi$
						hs	950 conf. mix of
							1, 3 Q_0 and a_{2u}, a_{1u}
							$\rightarrow d\pi$
						ls	1250 a_{2u}, $a_{1u} \rightarrow d\pi$

TABLE 2 (continued)

	N	B	$B(1,0)$	Q_0	$Q_v(1,0)$	$Q(3,0)$	CT bands
Met(OH)Mb high/low spin	353	413	391	578 ls 610 hs	541	 hs ls	488 $a_{2u'} \rightarrow d_{z^2}$ 625 a_{2u}, $a_{1u} \rightarrow d\pi$ 690 $a_{2u} \rightarrow d_{z^2}$ 727, 820 conf. mix of $_{1,3}Q_0$ $^{1,3}Q_0$ and a_{2u}, $a_{1u} \rightarrow d\pi$

[a] Taken from ref. 76. With the exception of certain CT bands, these PR values span the range 300–800. ls = low spin, hs = high spin.

$1,3Q_0$ and a_{2u}, $a_{1u} \rightarrow d\pi$). Met-myoglobin cyanide, a low spin complex, exhibits its $a_{2u} \rightarrow d_{z^2}$ CT band near 488 nm, and the a_{2u}, $a_{1u} \rightarrow d\pi$ bands near 1300 nm in the near IR. In addition, met-Mb CN exhibits an $e_g(\pi) \rightarrow d\pi$ band near 800 nm. This last CT band has been observed for all low spin ferric porphyrins; occurring near 690 nm for met-myoglobin azide [76]. Because of its z-polarization, Makinen and Churg [76] have postulated that the position of this band is a key to the degree of mixing of the metal and axial ligand orbitals. The positions of the $a_{2u} \rightarrow d_{z^2}$ and a_{2u}, $a_{1u} \rightarrow d\pi$ CT bands emphasize the importance of the metal d orbital splittings on the energies of the charge transfer bands. The larger crystal field splitting of the $t_{2g} - e_g$ orbitals of low spin porphyrins accounts for the low energy of the a_{2u}, $a_{1u} \rightarrow d\pi$ transition (1300 nm). This same transition occurs between 600 and 800 nm for high spin species. The t_{2g} orbitals of the low spin complexes are much lower in energy (Fig. 7).

Most high spin ferric porphyrin exhibit one or two charge transfer bands between 550 and 600 nm and between 600 and 800 nm [68,69,154,76], depending on the axial ligand attached. Other bands have been identified (see Table 2) at lower energy, but will not be discussed in detail in this paper. These charge transfer bands, assigned to porphyrin $\pi \rightarrow \mathrm{Fe}(d\pi)$ transitions, are usually intense due to mixing of the porphyrin $e_g\pi^*$ and metal d_{xz}, d_{yz} orbitals. In a high spin state the d_{xz}, d_{yz} orbitals are raised in energy, and are no longer degenerate. This allows the increased mixing and, hence, the higher intensity of the bands. Most low spin ferric porphyrin exhibit weak CT bands near 488 nm (Table 2), and generally stronger bands between 600 and 800 nm, with at least one band in the near IR. The band near 488 nm has been attributed to a porphyrin $a_{2u} \rightarrow$ metal d_{z^2} transition, while the bands between 600 and 800 nm are usually assigned to either a porphyrin a_{2u}, $a_{1u} \rightarrow$ Fe $d\pi$ or to a porphyrin $e_g(\pi) \rightarrow d\pi$ transition.

The absence of a band near 500 nm for hemin chloride in DMF is evidence for a change of spin state. In a non-coordinating solvent, hemin

chloride would remain high spin. However, this porphyrin exhibits different chemistry in coordinating solvents such as DMF or DMSO. Conductivity measurements by Brown and Lantzke have shown that while chloride dissociates in DMSO, it does not dissociate in DMF [78]. A similar chemistry results in acetone, where conductivity measurements have shown the chloride ion to dissociate [77]. The complex $[Fe(III)PPIX(DMSO)_2]^+ Cl^-$, is six coordinate and remains high spin, with an absorption band occurring near 500 nm (assumed to be the β-, or Q_v, band) [78]. This band was shown to vanish with time when DMF was substituted for DMSO and a new band grew in at 580 nm (Q_0). The reason for the disappearance of the Q_v band at 500 nm was attributed to the decomposition of DMF to a diethylamine complex, which easily displaced chloride ions and caused a change from high to low spin. The β- (Q_v) band associated with high spin complexes shifts from 500 to 540 nm and the α-band (Q_0) shifts from 540 to 580 nm as the spin state changes. The absence of a β-band near 500 nm for the hemin chloride DMF species suggests coordination of the diethylamine complex. There is enough evidence to rule out the possibility that Fe(III)PPIX(DMF) Cl or $Fe(III)PPIX(DMF)_2Cl$ are low spin.

The $\pi \rightarrow \pi^*$ bands (B, Q_0, Q_v, $B(1, 0)$) of ferrous porphyrins are all red shifted when the spin state of the metal changes from low to high spin. The CT bands of common origin, e.g., the Fe e_g ($d\pi$) $\rightarrow e_g$ (π^*) are also red shifted on going from a low to high spin state (Table 2). The $\pi \rightarrow \pi^*$ bands of ferric porphyrins are blue shifted when the metal spin state changes from low to high.

Ferric high spin complexes exhibit B bands near 400 and 380 nm, with the Q_v and Q_0 bands occurring near 500 and 545 nm, respectively. Low spin complexes exhibit B bands near 420 and 400 nm with Q_v and Q_0 shifting to 540 and 575 nm, respectively. The intensity of the Q_v band is independent of both the nature of the axial ligand and the metal oxidation state. The enhanced intensity of this band in both high and low spin porphyrins is attributed to vibronic coupling to the very intense B band [76]. However, the intensity of the Q_0 band is sensitive to these changes because it does not borrow from the B band [76,154]. The intensity of the Q_0 band is known to be dependent on the structure of the heme group [76]. The central iron atom is located in or near the plane of the porphyrin ring for most low spin porphyrins but is shifted out of the plane about 0.45 Å toward the axial ligand in high spin complexes. This shift causes the removal of degeneracy of the porphyrin $e_g\pi^*$ states, and perturbs the energy of the a_{2u} orbital, so that there is increased mixing with metal $d\pi$ orbitals. This results in increased intensity of the Q_0 band for high spin porphyrins. On the other hand, the Q_0 band is generally weak in low spin porphyrin (e.g. it is not observed in the normal UV–visible spectra of ferric cyanide or imidazole

TABLE 3

Electronic transitions for complexes of met-hemoglobin, hemeoctapeptide and proto-porphyrin-IX

High spin						
Complex	Soret	β	α	CT1	CT2	Ref.
met-HMGB(H_2O)	405	500	540 w	580 w	631	69
H8PT(H_2O) [a]	398	498	530	565	620	123
PPIX(Cl) [b]	396	–	550 m	570 m	615	123
Low spin						
Complex	Soret	CT1	β	α	CT2	Ref.
met-HMGB(N_3^-)	417	–	540	575	630 w	69
H8PT(N_3^-)	398	–	530	560	630	123
PPIX(N_3^-)	410	–	535	570	635	123
met-HMGB(HIm)	411	–	534	560	–	69
H8PT(HIm)	406	–	528	555	–	123
PPIX(HIm)	415	–	535	565	–	123
met-HMGB(CN^-)	419	–	540	–	–	69
H8PT(CN^-)	408	–	530	–	–	123
PPIX(CN^-)	435	–	555	–	–	123
PPIX(morp) [c]	405 415	–	525	553	660 w	123

[a] Solvent is a 50/50 (v/v) ethylene glycol–40 mM phosphate buffer.
[b] Solvent is dimethylformamide (0.033 mM). The spectrum for PPIX(Cl) in DMF also suggests the presence of diethylamine (see discussion).
[c] morp = morpholine; the disappearance of the band at 405 is followed by the appearance of a band at 415, as the ligand coordination number increases from one to two.

complexes), and is often buried beneath the more intense Q_v (β) band. The planar position of the iron atom causes less structural changes in a low spin state.

It is possible to observe transitions from porphyrin π-orbitals lower in energy than the a_{1u} or a_{2u} orbitals (Fig. 7). These transitions result in the appearance of several other bands: the *N* band, occurring near 350 nm; the *L* band, occurring near 260 nm; and the *M* band, occurring near 220 nm (Table 3). The positions of these bands are sensitive to the substituents on the porphyrin ring. The *N*, *L* and *M* bands are presumed to arise from transitions to $e_g\pi^*$ from the low lying π-orbitals, b_{2u}, $a_{2u'}$ and e_g. However, Makinen and Churg [76] have identified an a_{2u}; $b_{2u} \rightarrow e_g\pi^*$ CT band in this region. Therefore, identification of bands below 350 nm is not easy.

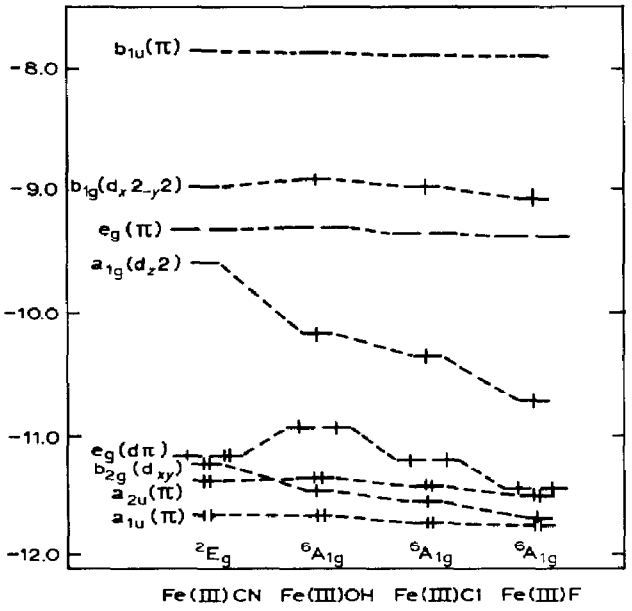

Fig. 8. Molecular orbital energy level diagrams for several hemin complexes (taken from M. Zerner, M. Gouterman and H. Kobayashi, Theor. Chim. Acta (Berlin), 6 (1966) 363).

Table 3 shows that as the ligand becomes a better π-acceptor, the position of the Soret band is shifted to the red. This band shifts from 395 nm for chloride to 410 for the azide to 435 for the cyanide protoporphyrin species. The exact reasons for the red shift are not entirely known, but the generally accepted theory is perturbation of the energy of the ring π-orbitals by the axial ligands [68,69,72,73]. For example, π-acceptor ligands such as cyanide or imidazole would lower the energy of the ferric $d\pi$ orbitals ($d_{xz,yz}$) by draining electron density away from the metal. The crystal field splitting (i.e., e_g–t_{2g} separation (see Fig. 8)) would increase compared to the high spin case (e.g., with chloride at the axial site). Retrodative bonding between the metal and ligand should lower the separation between the ring π and π^* orbitals, as the metal becomes more electronegative toward the porphyrin ring.

Charge transfer transitions are expected to occur at higher energy for the π-donating ligands such as fluoride because such ligands would increase the electron density at the metal center. This would then require more energy for an electron transfer from the porphyrin ring to the metal. Alternatively, when π-acceptor ligands are attached to the metal, they are able to drain electron density through retrodative bonding, and the metal becomes more electronegative toward the porphyrin ring. Under these conditions, electron transfer would be expected to occur at much lower energy.

The positions of the charge transfer bands presented in Table 3 show this trend. In the hemeoctapeptide species, the pure aquo complex (high spin) exhibits charge transfer bands near 620 nm, but occurs near 630 nm for the low spin complex. The position of the $a_{2u} \rightarrow d_{z^2}$ (porphyrin → Fe) CT band is slightly affected by the strength of the axial ligand for ferric low spin complexes (Table 2). The energies of this band are identical for met-myoglobin cyanide and azide complexes, but the band shifts to 690 nm for met-MYGB hydroxide and is found near 666 nm for the high spin met-aquo species. This is likely related to *d*-orbital splitting affecting the energy of the d_{z^2} orbital. However, there are no CT bands between 600 and 750 nm for cyanide porphyrins of met-myoglobin, hemoglobin, hemeoctapeptide, or protoporphyrin-IX. Strong field ligands such as cyanide significantly alter the energies of the t_{2g} (d_{xz}, d_{yz}, d_{xy}) orbitals. Met-myoglobin complexes containing hydroxide or azide ligands are of mixed spin states ($S = 1/2 \leftrightarrow S = 5/2$), and the a_{2u}, $a_{1u} \rightarrow d\pi$ (porphyrin → Fe) CT bands are found at both 625 and 1250 nm, indicating both a low and high spin component. This same band is found near 1300 nm for the pure low spin cyanide complex. The position of this band is a marker for spin state changes, because it reflects the energies of the *d* orbitals. Kassner and co-workers have identified spin equilibrium behavior for both hemeoctapeptide azide and hydroxide complexes [25]. Owens and O'Connor have also found such behavior to exist for protoporphyrin-IX azide in dimethylformamide [158]. Morishima and Neya [122] have also identified a spin equilibrium state for protoporphyrin-IX azide in dimethylsulfoxide. The electronic transitions are similar for all these complexes. On the basis of the assignment of the met-myoglobin high spin species we assign the protoporphyrin and hemeoctapeptide high spin CT band at 570–580 nm to an $a_{1u} \rightarrow d\pi$ transition (porphyrin–Fe) and the band at 631 nm to an $a_{2u} \rightarrow d\pi$ transition (porphyrin → Fe).

(iii) d–d *Transitions*

This discussion would not be complete without some brief discussion of $d \rightarrow d$ transitions. In D_{4h} symmetry, all $g \rightarrow g$ transitions are forbidden and are observed only when the symmetry is removed, for example by axial binding of two different ligands. The distortion could be from $D_{4h} \rightarrow C_{2v}$, if unsymmetrical ligands are attached [79]. (See Table 1 for symmetry correlation diagrams.) For high spin hemins, a second hurdle arises, since all transitions are both symmetry and spin forbidden. Therefore $d \rightarrow d$ transitions for high spin hemins have never been definitely observed spectroscopically. The *d–d* transitions in low spin hemins are spin allowed but symmetry forbidden. These transitions also become allowed by a reduction in symme-

try. Makinen and Churg have used PR data and IEH calculations for several met-myoglobin complexes to identify several $d \rightarrow d$ transitions occurring between 250 and 350 nm. If this is true, it is highly unlikely that these bands would be observed in a normal UV–visible absorption spectrum since they would be buried beneath more intense porphyrin $\pi \rightarrow \pi^*$ and CT transitions. Eaton and coworkers [153] have suggested the appearance of $d \rightarrow d$ transitions in the visible region between 500 and 700 nm for deoxy- and carbonyl-hemoglobin complexes. They proposed $d_{x^2-y^2} \rightarrow d_{xy}$ and $(d_{xz}, d_{yz}) \rightarrow (d_{z^2}, d_{xy})d$–$d$ transitions (e.g. $^1A_1 \rightarrow {}^1A_2$ and $^1A_1 \rightarrow {}^1E$, respectively). However, these assignments have been challenged by Makinen and Churg [76]. The question of $d \rightarrow d$ transitions remains unresolved [80–83].

C. VIBRATIONAL SPECTROSCOPY

(i) Porphyrin vibrations

The vibrations of the porphyrin ring may be of two kinds: (1) out-of-plane vibrations, including bending of the in-plane bands; and (2) in-plane vibrations. If the peripheral substitutes are assumed to be point masses, for example as in free base porphin, and a metal is placed in the center, a porphyrin complex has 105 vibrations. These vibrations consist of 71 in-plane vibrations and 34 out-of-plane vibrations [83–85].

The local symmetry of the iron(III) ion is planar with a D_{4h} assignment. The 71 in-plane vibrations span the following irreducible representation: $\Gamma_{ip} = 9\ A_{1g}$, $8\ A_{2g}$, $9\ B_{1g}$, $9\ B_{2g}$ and $18\ E_u$ (ip = in-plane). Of these 71 vibrations, only the 18 E_u modes are IR active. All others, except A_{2g}, are Raman active (9 polarized A_{1g} bands, 18 depolarized B_{1g} and B_{2g} bands, and 8 anomalously polarized A_{2g} bands). The internal basis sets used to generate the symmetry of the in-plane modes are shown in Table 4 and Fig. 9, where 98 vibrations are totalled; 27 of these are redundant and are so indicated.

None of the symmetrical stretches involving C–H, C_b–C_b, C_a–N, C_a–C_b, C_a–C_m or C_b–S (S = a peripheral substituent) is IR active as they span A_{1g} and possess small dipole moment derivatives. Neither are the Fe–N symmetrical stretches active in the IR. These symmetrical stretches have, however, been identified and assigned using resonance Raman techniques, which have proved to be powerful tools in the structural diagnosis of hemins [7,86–93].

It is known that hemes and their proteins contain sets of bands that are in resonance with the Soret and α, β electronic transitions [86–89]. Raman excitation into the Soret region is associated with Franck–Condon type overlap factors (A-type band) [87,89] and are thus polarized. These A-type Raman transitions involve the totally symmetric A_{1g} vibrations and connect

TABLE 4

Internal basis set for the vibrational modes of a D_{4h} core metalloporphyrin

Mode	A_{1g}	A_{2g}	B_{1g}	B_{2g}	E_u
νC_mH	1	0	0	1	1
νC_bC_b	1	0	1	0	1
νC_aC_m	1	1	1	1	2
νC_aN	1	1	1	1	2
νC_aC_b	1	1	1	1	2
νC_bS [a]	1	1	1	1	2
νMN	1	0	1	0	1
δC_aC_mH	0	1	1	0	1
δC_bC_bS	1	1	1	1	2
$\delta C_aC_mC_a$	1	0	0	1	1
$\delta C_bC_bC_a$	1	1	1	1	2
$\delta C_bC_aC_m$					
δC_bC_aN	2	2	2	2	4
δC_mC_aN					
δC_aNC_a	1	0	1	0	1
δC_aNM		1		1	2
δNMN	1	0	0	1	1

See Fig. 9 for atom labels. The in-plane vibrational modes $= 9A_{1g} + 8A_{2g} + 9B_{1g} + 9B_{2g} + 18E_u$.

Cyclic redundancies $= 5A_{1g} + 2A_{2g} + 3B_{1g} + 3B_{2g} + 7E_u$.

ν = X–Y bond stretching.

δ = X–Y–Z angle bending.

[a] S = a ring substituent.

(Taken from A.B.P. Lever and H. Gray (Eds.), Iron Porphyrins, Part Two, Elsevier, New York, 1983, pp. 89–159).

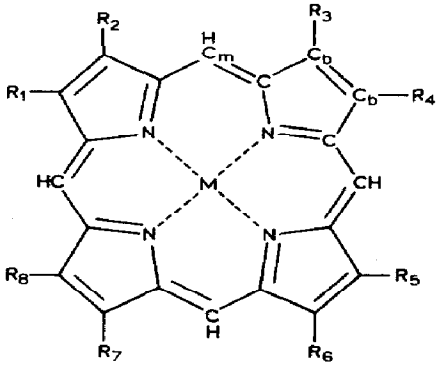

Fig. 9. Structural diagram for the porphyrin ring showing the atom numbering scheme. For hemin compounds, R_2 and R_4 = vinyl groups. R_6 and R_7 = propionic acids; R_1, R_3, R_5 and R_7 = methyl groups (taken from ref. 2).

the ground state to the excited state through changes in the energy of the excited state. Thus, those transitions not involving origin displacement are enhanced by excitation near the Soret region (370–440 nm).

Excitation into the Q band region, spanning the α, β electronic transition (500–600 nm) are governed by the Herzberg–Teller mechanism [84,89] and are either depolarized or anomalously polarized. These transitions, known as type B, involve the non-totally symmetric A_{2g}, B_{1g} and B_{2g} modes, which arise via vibronic coupling. Vibronic coupling enables otherwise inactive vibrations by coupling to an electronic transition of suitable symmetry [91]. Although these latter transitions (type B) may have any symmetry spanned by the direct product of the two electronic transitions ($E_u \times E_u = A_{1g}$, A_{2g}, B_{1g}, and B_{2g}), it is known that A_{1g} type models are clearly ineffective in mixing vibrational and electronic modes [84].

The B_{1g} and B_{2g} modes are depolarized, while the A_{2g} mode, disallowed in Raman spectroscopy under the veil of D_{4h} symmetry, are either anomalously or inverse polarized due to their association with antisymmetric scattering tensors ($\alpha_{xy} = \alpha_{yz}$) [87,95,96]. The A_{2g} modes become active in the resonance Q band region and are identified on the basis of their anomalously polarized ratio, $3/4 < P_1 < \infty$ or their inverse polarization ratio $P_1 = \infty$. P_1 is the polarization ratio for the intensity of the transition perpendicular to the plane of incident radiation compared to the intensity of the transition parallel to the plane of incident radiation. Polarized modes (A_{1g}) in the Soret region have $P_1 < 3/4$, depolarized modes in the visible region (Q region) have $P_1 = 3/4$ (B_{1g} and B_{2g}), anomalously polarized modes in the visible have $P_1 > 3/4$ and may have $P_1 = \infty$, but for those cases where $P_1 = \infty$ such modes are also inversely polarized.

The E_u modes involve transitions associated with asymmetry about the central metal. They are not expected to be active in the Raman. However, enabling mechanisms, such as symmetry lowering or vibronic coupling, could induce Raman activity in these otherwise exclusively IR modes. The selection rules which govern IR and Raman activity, as well as the polarization for Raman bands, are explained in a variety of texts [94,97–99]. When a band is seen in either the IR or Raman which is disallowed by the selection rules, its origin may be traced to one or more of the enabling mechanisms mentioned above. This explains the appearance of the E_u mode in the Raman spectra of protoporphyrin-IX. For comparison, the IR active E_u modes are shown in Table 5. All 71 of the in-plane modes have been described and drawn by Abe and coworkers [100], in which all the force constants were tabulated using a Urey–Bradley force field in one of the most deliberate and elegant normal coordinate analysis ever done. The entire vibrational spectrum for both the IR and Raman modes were assigned. The calculated frequencies have been universally supported by experiment [69,86–93].

TABLE 5

E_u IR frequencies for PPIX-Cl

Mode	Frequency	Substituent mode
	1735	
	1705	ν_{COOH}
	1626	$\nu_{C=C}$
C_aC_m	1525	
C_aC_m	1458	
C_aC_b	1441	
C_aN	1381	
C_aN	1338	δ_s=CH_2
C_aN	1301	δCH=
C_mH	1280	
C_bS	1150	
C_bS	1122	
C_bS	1087	δ_{as}=CH_2
C_bS	1004	CH=
C_aN	998	
C_bS	920	γ_s=CH_2
C_mH	848	
C_bS	712	

See Figs. 9 and 10 for atom labels. All vibrations unless otherwise indicated are stretching frequencies. δ = bending, γ = rocking vibrations; s = symmetric, as = asymmetric. (Taken from ref. 102.)

TABLE 6

Local-mode contributions to the out-of-plane normal modes of a D_{4h} metalloporphyrin with point mass pyrrole substituents

Mode [a]	A_{1u}	A_{2u}	B_{1u}	B_{2u}	E_g
γC_mH		1	1		1
pyr fold(s)		1		1	1
pyr fold(as)	1		1		1
γC_bS	1	1	1	1	2
γC_aC_m		1	1		1
pyr tilt		1		1	1
pyr swivel	1		1		1
pyr trans.		(1) [b]		1	(1) [c]
γNM		1			
Total	3	6	5	4	8

[a] See Fig. 10 for descriptions (taken from ref. 84). [b] Molecular translation about z. [c] Molecular rotations (R_x, R_y).

There are a total of 34 out-of-plane vibrations (Γ_{oop}) for a typical metalloporphyrin: $\Gamma_{oop} = 3\ A_{1u}$, $6\ A_{2u}$, $5\ B_{1u}$, $4\ B_{2u}$, and $8\ E_g$. Of these 34 vibrations, only the $6\ A_{2u}$ modes are IR active; and only the $8\ E_g$ modes are Raman active. Out-of-plane Raman active vibrations are not understood as well as the in-plane vibrations because there is no electronic enhancement of these non-planar porphyrin modes from resonance with the $\pi \rightarrow \pi^*$ transitions of the B and Q bands. Such a restriction is removed, however, by vibronic mixing of in-plane (E_u) and out-of-plane (A_{2u}) electronic transitions: $E_u \times A_{2u} = E_g$. All out-of-plane modes occur below 1000 cm^{-1}. The basis set used to generate the out-of-plane modes is shown in Table 6 and Fig. 10. Most are "u" type vibrations, yet only the A_{2u} fits all requirements for IR activity. The positions of the peripheral vinyl modes have also been assigned (Fig. 11).

Since only a few modes are active in the IR and even fewer modes involve the very important metal sensitive vibrations, their Raman spectra have become significant. A complete list of these frequencies is shown in Table 7 for hemin chloride, hemin diimidazole and the bis-DMSO complex of

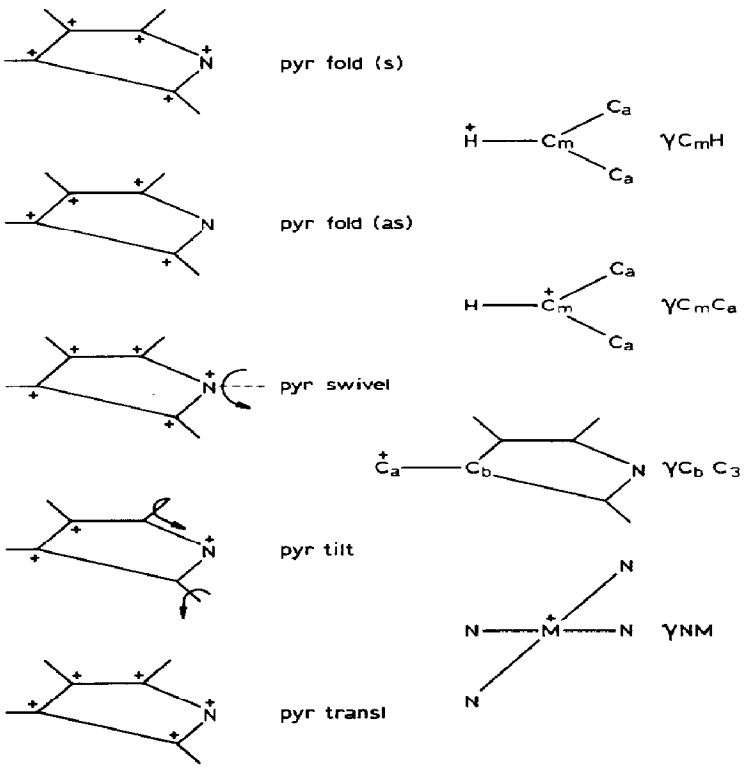

Fig. 10. Schematics of the out-of-plane displacement coordinates for the out-of-plane modes (taken from ref. 84).

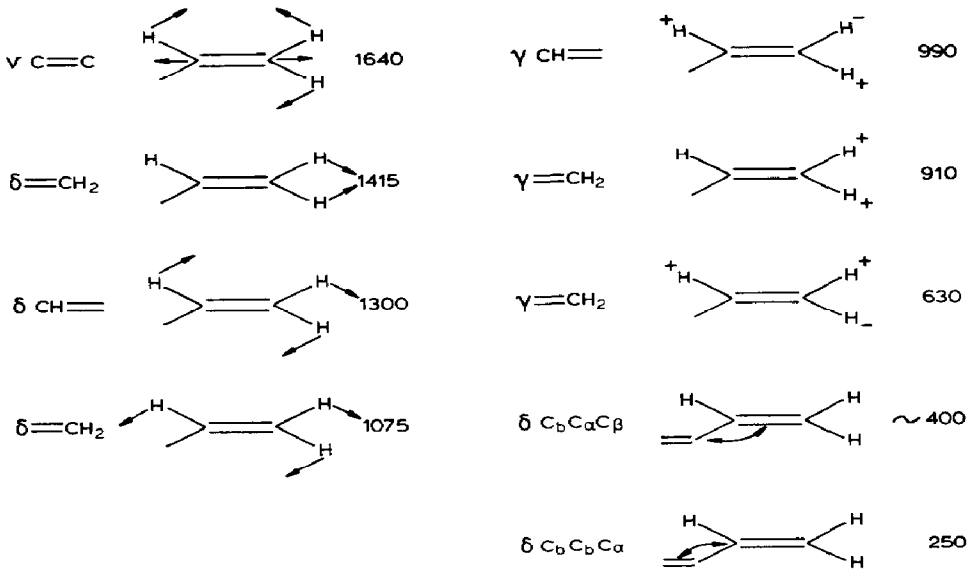

Fig. 11. Schematics and frequencies for the vinyl modes of PPIX-Cl (taken from ref. 102).

hemin. The positions of the vibrations for [Fe(II)PPIX(2-MeIm)] are also included in Table 7 for comparison with the ferric complexes.

(ii) Metal–ligand vibrations

The most important of the vibrational features pertinent to the characterization of hemin and its derivatives is the Fe–L stretch (L = N_3^-, CN^-, Im^-, etc.). Vibrational spectra may be used to characterize 5-coordinate hemin complexes, as in hemin azide [Hemin (N_3)], and 6-coordinate hemin complexes, as in [Hemin $(CN)_2]^-$ or [Hemin $(HIm)_2]^+$.

The 6-coordinate hemin diimidazole complex may be closely approximated as belonging to point group D_{4h}. The Fe–L_2 symmetric stretch belongs to the A_{1g} representation and is Raman active, but IR forbidden. However, there is no mechanism for enhancement of the Raman modes, because both electronic bands (B, or Soret, and Q, or α and β bands) are in-plane $\pi \rightarrow \pi^*$ transitions and the Fe–L_2 stretches are clearly out-of-plane modes.

These 6-coordinate complexes exhibit both symmetric and asymmetric stretching out-of-plane modes. The asymmetric Fe–L_2 stretch carries A_{2u} symmetry, and is fully allowed in the IR, but disallowed in the Raman, because of its "u" type symmetry. It could, however, become activated because of symmetry lowering; for example the two imidazoles in [Fe(III)(Proto-IX)$(HIm)_2$]Cl are not equivalent [3], and the D_{4h} symmetry is

TABLE 7

Resonance Raman frequencies (cm^{-1}) for PPIX complexes

Mode	$Im_2Fe(3+)$	$Im_2Fe(2+)$	$ClFe(3+)$	$(DMSO)_2Fe(3+)$	(2-MeIm)Fe(2+)
C_aC_m	1640	1617	1617	1610	1604 (B_{1g})
C_bC_b	1602	1604	1591	1580	1583 (E_u)
C_aC_m	1586	1583	1571	1560	1550 (A_{2g})
C_bC_b	1579	1584	1570	1559	1562 (A_{1g})
C_bC_b	1562	1539	1553	1545	1547 (B_{1g})
C_aC_m	1554	1560	1533	1518	1521 (E_u)
C_aC_m	1502	1493	1491	1480	1471 (A_{1g})
C_aC_b	1402	1390	1403	1392	1392 (B_{2g})
C_aN	1399	1392	1403	1389	1401 (A_{2g})
C_aN	1373	1359	1373	1370	1357 (A_{1g})
δC_mH	1306	1305	1309	1313	1302 (A_{2g})
δC_mH	1230	1225	1228	1225	1227 (B_{1g})
C_aN	1125	1125	1127	–	1122 (A_{2g})
C_aN	997	995	–	–	999 (E_u)
C_bS	951	925	–	–	921 (E_u)
$\delta C_aC_mC_a$	804	819	806	786	787 (A_{1g})
δC_bS	791	791	–	–	(B_{2g})
δC_aNC_a	749	748	722	–	752 (B_{1g})
C_bS	714	717	694	–	714 (E_u)
δC_bC_aN	677	675	675	677	676 (A_{1g})
δC_bS	605	588	–	–	585 (E_u)
$\delta C_aC_bC_b$	561	558	555	–	548 (E_u)
pyr fold	510	507	–	–	510
pyr fold	495	488	492	495	495
pyr fold	425	426	410	–	–
pyr tilt	–	254	–	–	255
pyr tilt	–	236	237	–	–
ν_sFe–L	199	201	–	–	–

Values taken from ref. 102. All modes are stretching unless otherwise indicated. δ = out-of-plane vibrations. The skeletal configurations are defined in Figs. 9 and 10.
ν_s = symmetric M–L stretch.

lost. Therefore, both the A_{1g} symmetrical Fe–L_2 stretch and the otherwise inactive A_{2u} asymmetric stretch may be observed and enhanced by coupling to a $\pi \rightarrow \pi^*$ porphyrin electronic transition when there is a relaxation of the selection rules caused by the removal of the center of symmetry.

Symmetric and asymmetric bands have been located for several complexes of interest and these are shown in Table 8. It should be pointed out, however, that no Fe–L_2 stretches have been identified for $[Fe(III)(Proto\text{-}IX)(CN)_2]^-$ either in the IR or Raman [88]. The expected bands are buried in the multitude of porphyrin bands occurring in the same regions where Fe–L_2 stretches would appear. Neither have axial stretching modes been

TABLE 8

Metal stretching frequencies for some porphyrin and protein complexes

Mode	Frequency (cm^{-1})	Molecule	Ref.
For [Imidazole–Fe(2+)–X] species(low spin)			
Fe–O_2	567	HMGB–O_2	102
Fe–O_2	561–567	O_2(N-MeIm)Fe(2+)$TP_{iv}PP$	103–105
Fe–O_2	572	MYGB–O_2	106
Fe–NO	553	HMGB–NO	107
Fe–CO	507	HMGB–CO	108
Fe–ImH	271	MYGB–O_2	109
For [Imidazole–Fe(3+)]–X^- species			
Fe–N_3	413	HMGB–N_3	110
Fe–N_3	411	MYGB–N_3	111
Fe–OH	497	HMGB–OH	110
Fe–ImH	248	MYGB–H_2O	112
For $[Fe(3+)–X]^-$ (5-coordinate)			
Fe–S(cys)	351	CYT–P450	113
Fe–F	606	OEP–F	114
Fe–Cl	360	OEP–F	114
Fe–I	245	OEP–I	114
Fe–N_3	421	OEP–N_3	114
Fe–N_3	412	PPIX–N_3	123
Fe–Cl	357	PPIX–Cl	123
For $[L–Fe(3+)–L]^n$ species (low spin) $n = 0$ or -1			
Fe–$(ImH)_2$	200(s)	$PPIX(ImH)_2^+$	92
Fe–$(ImH)_2$	377(asym)	$OEP(ImH)_2^+$	114
Fe–$(ImH)_2$	377(asym)	$PPIX(ImH)_2^+$	115

HMGB = hemoglobin, MYGB = myoglobin, CYT-P450 = cytochrome-P450, PPIX = protoporphyrin-IX, OEP = octaethylporphyrin, $TP_{iv}PP$ = "picket-fence" porphyrin, s = symmetric metal–ligand stretch, asym = asymmetric metal–ligand stretch, ImH = neutral imidazole, N_3 = azide.

identified for $[Fe(III)(Proto\text{-}IX)(DMSO)_2]^+$. Five coordinate complexes of hemin possess C_{4v} symmetry and the M–L stretch spans A_1. It is found at higher frequency than both the symmetric and asymmetric $M–L_2$ stretches in six coordinate hemins, proving that the higher coordination number generally decreases the frequency.

The M–N(pyrrole) bond length increases [53]: $[(ImH)_2Fe(III)] < [(ImH)_2Fe(II)] < [(DMSO)_2Fe(III)] < [(Cl)Fe(III)] < [(2\text{-}MeImH)Fe(II)]$ for the tetraphenyl series. The Fe(III)Proto-IX series would be expected to follow this same order. Table 9 lists some bond lengths for several iron

TABLE 9

Bond lengths for some iron porphyrins

Molecule	Spin/Coord. No.	C_t–N	Fe–N(pyr)	Fe–L	Ref.
Fe(2+)TPP	IS/4	1.972	1.972	–	116
$(OClO_3)$Fe(3+)TPP	IS/5	1.979	1.997	2.025	117
$[(ImH)_2$Fe(3+)TPP$]^+$	LS/6	1.989	1.989	1.991	3
$[(1\text{-MeIm})_2$Fe(3+)PPIX$]^+$	LS/6		1.990	1.977	48
$[(1\text{-MeIm})_2$Fe(2+)TPP]	LS/6	1.997	1.997	2.014	118
(Cl)Fe(3+)TPP	HS/5	2.012	2.049	2.192	119
(Cl)Fe(3+)PPIX	HS/5		2.062	2.218	41
(2-MeIm)Fe(2+)TPP	HS/5	2.044	2.086	2.161	120
$[(TMSO)_2$Fe(3+)TPP$]^+$	HS/6	2.045	2.045	2.069	65
O_2(N–MeIm)Fe(2+)TP_{iv}PP			1.98av	1.750	121

All bond lengths are in Ångstrom units.
IS = intermediate spin; $S = 3/2$ for Fe(3+) or 2/2 for Fe(2+).
HS = high spin; $S = 5/2$ for Fe(3+) or $S = 4/2$ for Fe(2+).
LS = low spin; $S = 1/2$ for Fe(3+) or $S = 0$ for Fe(2+).
TPP = tetraphenylporphyrin, PPIX = protoporphyrin, TMSO = tetramethylsulfoxide, MeIm = methyl imidazole.
C_t–N = distance from the center of the porphyrin ring to the pyrrole nitrogen of the porphyrin ring. Fe–N = distance from the metal to the pyrrole nitrogen of the porphyrin ring. Fe–L = distance from the metal to the ligand.

porphyrin complexes. The M–N(pyrrole) bond order increases in the reverse order. The M–N(pyrrole) stretching frequencies increase with decreasing bond length and increase with increasing bond order. This increase in M–N(pyrrole) stretching frequency can be attributed to diminishing Fe → porphyrin π back donation.

It is not surprising to find that the ferroprotoporphyrins have generally lower M–N(pyrrole) frequencies, because the larger size of the Fe^{2+} cation compared to its 3+ state forces two effects: (1) a longer M–N(pyrrole) bond due to a less than optimum orbital overlap; (2) the reduced effective charge on the 2+ state introduces "softness" [60–62] into the cation and it becomes less electronegative toward the porphyrin ring.

Since ferroprotoporphyrin complexes usually do not coordinate anionic ligands, a typical high spin complex is represented by DMF [101]. That Fe(II)–(DMF) porphyrin complexes have higher M–N(pyrrole) frequencies than high spin [Fe(II)(2-MeImH)] complexes is attributed to the smaller pK_a. DMF is a poorer base. 2-MeImH is not a good π-acceptor but is a good base. Although the M–L bond is stronger for the high spin *N*-substituted imidazole complex, the M–N(pyrrole) bond distance is longer as a consequence of a larger metal electron density shift onto the porphyrin ring (*cis* effect). The Fe(II)–CO porphyrin complex would be expected to have

shorter M–N(pyrrole) bonds because CO has π-acceptor orbitals which can accept electron density from the metal by retrodative bonding, and less density would be shifted to the porphyrin ring.

Analogous arguments can be made for 6-coordinate ferric low spin and 6-coordinate ferric high spin species. In 5- and 6-coordinate high spin complexes, the M–N(pyrrole) bond length is affected by both σ- and π-interactions. The radial expansion is attributed in part to increased population of the $d_{x^2-y^2}$ orbital (a σ-effect) which reduces overlap of the metal and ligand σ-bonding orbitals through electrostatic interactions. The shorter length of M–N(pyrrole) bonds in low spin complexes can likewise be partially attributed to σ-effects: specifically, the depopulation of the $d_{x^2-y^2}$ antibonding orbitals and subsequent ruffling of the pyrrole ring. π-effects are of two types: metal $d(\pi) \leftrightarrow$ ligand (π) and metal $d(\pi) \leftrightarrow$ N(π)pyrrole. The lower basicity of the weak field ligand is a factor which does not lessen M $\rightarrow$ N(pyrrole) π-donation. However, strong field ligands possess the capability to remove π-electron density from the metal through retrobonding.

In 5-coordinate high spin complexes, the Fe atom moves out of the plane toward the ligand, and the 4 pyrrole nitrogens follow (doming). This has the effect of shrinking the porphyrin ring around the metal and the Fe–N(pyrrole) bond length decreases comparably. Generally, for high spin complexes containing π-donating ligands, the Fe $\rightarrow$ porphyrin ring π donation increases as the Fe–L bond order increases. In 6-coordinate high spin hemins, the metal is located very near or in the plane of the porphyrin ring. Therefore the M–N(pyrrole) bond length increases as the $d_{x^2-y^2}$ antibonding orbital is populated and inhibits good orbital overlap with the ring orbitals.

Some axially bound ligands have very identifiable vibrational modes, particularly π-bonded ligands (L = CN^-, CO, N_3^-, O_2, etc.) Others may possess one or more vibrational modes distinct from the hemin porphyrin but are discerned only with difficulty. For example, imidazole complexed to hemin is not easily discerned from its unbound spectrum because ligation causes little or no perturbation of bond strength, due to the size of the imidazole ring and delocalization of the electron donor pair.

This is not the case for the smaller anionic and neutral unsaturated ligands. These ligands undergo a bond strength perturbation upon complexation with hemin. When hemin is complexed by ligands that possess internal multiple bonds, it is generally found that the stronger the M–L bond, the weaker the internal bond order of the ligand. Therefore, the bound and unbound ligands should exhibit quite different stretching and/or bending frequencies. An extensive survey of the unbound and bound vibrations for ligands of immediate importance is shown in Table 10, using both the IR and Raman techniques.

TABLE 10

Bound and unbound stretching frequencies for some common porphyrin-ligand complexes

Ligand	Porphyrin	Medium	Bound	Unbound	Ref.
Azides					
azide	DPDME	KBr pellet	2055a	–	43
azide	DPDME	$CHCl_3$	2060a	–	41
azide	PDME	KBr pellet	2065a	–	43
azide	PDME	$CHCl_3$	2065a	–	43, 122
azide [a]	PDME	dry pyr	2010 2045a	–	43
azide [a]	PPIX	DMSO	2045 2054a	–	122
azide	PPIX	KBr pellet	2060a	–	113
azide	OEP	KBr pellet	2060a 1327s 629b	–	114
azide	NaN_3	$CHCl_3$	–	–	
azide	NaN_3	dry pyr	–	2170	43
azide	NaN_3	pyr/water	–	2025	43
azide	NaN_3	DMSO	–	1999	122
azide	NaN_3	KBr pellet	–	2040 2100	[b]
Cyanides					
cyanide [c]	DPDME	pyr/water	2110 2125	–	43
cyanide	PDME	pyr/water	2110 2125	–	43, 124
cyanide	KCN	pyr/water	–	2075	43
cyanide	KCN	water	–	2078	43
cyanide	AgCN	KBr pellet	–	2130	[b]
Oxygen					
oxygen	HMGB–O_2	–	1107	–	102
oxygen	$TP_{iv}PP$	–	1159	–	103–105
oxygen	oxyhemerythrin		844	–	43
oxygen	dioxygen	–	–	1580	125
oxygen	superoxide	–	–	1097	125
oxygen	peroxide	–	–	802	125
Carbon monoxide					
CO	PDME	$CHCl_3$	1975	–	124
CO	CO	gas	–	2143	124
Imidazole					
Imidazole	OEP	KBr pellet	3240 1505 1329 658	–	114

TABLE 10 (continued)

Ligand	Porphyrin	Medium	Bound	Unbound	Ref.
Imidazole	Imidazole	KBr pellet	–	3240 1505 1329 658	114

DPDME = deuteroporphyrin dimethyl ester, PDME = protoporphyrin dimethyl ester, PP = protoporphyrin, OEP = octaethylporphyrin, DMSO = dimethyl sulfoxide; $TP_{iv}PP$ = tetrapivaloylamide protoporphyrin-IX.

a = asymmetric stretch, s = symmetric stretch, b = bending.

[a] The authors have indicated a high spin/low spin state for these systems; the higher frequency represents the high spin state in all cases. [b] Sadtler's Index of Infrared Spectra. [c] The two peaks represent monocyano (2125) and dicyano (2110) species.

There are virtually no bands seen in the region 1900–2600 cm^{-1} for the IR spectra of hemins complexed to axial ligands that do not contain internal multiple bonds. Fortunately, it is precisely this region which is most diagnostic for complexation of small unsaturated systems because most of them exhibit IR active asymmetric stretching modes therein. Table 10 shows the N_3^- stretch at ~ 2060 cm^{-1} [30–33] and the CN stretch at ~ 2042 cm^{-1} for most porphyrins [43,71,124]. For comparison, the other modes are well removed from the asymmetric stretch. For example, the N_3^- symmetric stretch occurs near 1330 cm^{-1} and the bending mode near 629 cm^{-1}. Table 8 shows the Fe–N_3 stretch at 420 cm^{-1}.

The unique difference between cyanide and azide, carbon monoxide, or oxygen, is that the internal frequency of the cyanide shifts to a higher value upon coordination [43,48], whereas bound complexes of the others shift their internal vibrations to lower values (Table 10). The symmetric stretch for free oxygen is found in the Raman near 1580 cm^{-1} [125], while the center of symmetry excludes the appearance of this band in the IR. The asymmetric stretching frequencies for complexed oxygen appear in the IR due to a perturbation of its molecular symmetry from a linear to a bent geometry. The position of the O–O stretch in a typical non-porphyrin complex (e.g. $Ir(CO)(Cl)[P(C_6H_5)_3]_2(O_2)$) is near 860 cm^{-1} [126]. A similar stretch occurs near 1157 cm^{-1} in the "picket fence" protein model, $[O_2(N\text{-}MeIm)Fe(II)TP_{iv}PP]$ [104]. A band occurs near 1107 cm^{-1} for oxyhemoglobin [102], and has led many to propose a superoxide model for oxyhemoglobin, $[Fe^{3+}–O_2^-]$ [128–130]. The superoxide O–O stretch is known to occur near 1100 cm^{-1} and the peroxide O–O stretch occurs near 840 cm^{-1} [125]. However, the superoxide O–O stretch in porphyrins has been shown to arise from a vibronically coupled splitting of a fundamental Fe–O stretch [102] at 567 cm^{-1}, and is therefore not of pure O–O origin [157]. The

absence of a pure O–O vibration in the vicinity of the superoxide region (1100 cm^{-1}) has cast doubt on the Fe^{3+}–O_2-ionic charge model. It is probable that the band at 1157 cm^{-1} in the "picket fence" porphyrins also has a contribution from the Fe–O stretch at 567 cm^{-1}. The O–O stretch occurs at 844 cm^{-1} in oxyhemerythrin [127]. This represents an extreme shift in bond order for the internal vibrational modes of bound O_2.

The Fe–O_2 stretch occurs at 504 cm^{-1} for oxyhemerythrin [127]. The Fe–O_2 bond geometry has been shown to be such that the oxygen binds the iron "end-on" [128,129]. The electronic make-up of the Fe(II)–O_2 bond in oxyhemoglobin has been suggested to be of a Fe(III)–O_2^- type structure, with an almost complete electron transfer from the divalent metal to dioxygen [128–130]. This creates ionicity in the bond, with the metal assuming a trivalent oxidation state and the oxygen gaining an electron to become a superoxide ion. Makinen and Churg [155,156] have suggested that a superoxide formulation is in error. They proposed a low spin ($S = 0$) d orbital arrangement of the metal, with the oxygen in a spin paired singlet $^1\Delta g$ arrangement. This model is essentially that originally proposed by Pauling and is entirely covalent. They based their covalent model on the assignment of a porphyrin (π) $\rightarrow O_2(\pi g)$ transition occurring in the near infrared. They also reasoned that a molecular orbital description of the $Fe^{3+}O_2^-$ model would necessitate a diamagnetic ground state of the form

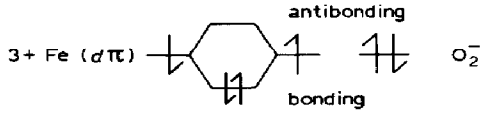

since the singly occupied metal and oxygen orbitals would pair in the low energy bonding orbital. It has been known for some time that the ground state of oxyheme is totally diamagnetic [157], with no evidence of paramagnetism. Since the ground state requires tight coupling of ions in the $Fe^{3+}O_2^-$ model, the end result is the same as that of a covalent system, with the oxygen ligand displaying σ- and π-bonding with the metal center. The controversy over the electronic make-up of the Fe–O_2 bond appears to be favoring the Pauling model; others still prefer the superoxide model.

The similarity of the Mössbauer spectra of low spin ferrous and ferric complexes suggested that low spin ferric complexes are better models for oxyhemoglobin than high spin ferric complexes. The data suggest some charge transfer from the ferrous iron of oxyhemoglobin to the oxygen atom. While there is a one-electron transfer in oxyhemoglobin, there is a two-electron transfer in oxyhemerythrin, as the O_2 molecule becomes the O_2^{2-} peroxide ion. The increasing population of the oxygen molecular antibonding orbitals from the metal $d\pi$ orbitals is therefore reflected in the

positions of the vibrations. The decrease in position for the O–O internal stretching frequency in the series, dioxygen > superoxide > peroxide, represents a decrease in bond order as the π^* antibonding orbitals are progressively filled. Specifically, the O–O bond undergoes a decrease in covalency on going from dioxygen to the superoxide to the peroxide, while the Fe–O_2 bond undergoes an increase in bond order.

It is only with oxygenated porphyrins that this type of behavior has been observed, and serves as an uncanny reminder that metal–oxygen chemistry in proteins is complex and unique. Even though it is known that oxygen is as good a π-acid ligand as cyanide, carbon monoxide, and nitrous oxide, and these last ligands will poison the protein binding site for oxygen, such complex protein chemistry has not been observed for any of these other π-acid ligands.

Protohemin solutions of cyanide show IR bands near 2112, 2125, and 2073 cm^{-1}, representing the dicyano, monocyano, and unbound cyanide species, respectively [43]. CO complexes of hemins show similar differences in bound and unbound spectra [43]. Imidazole has several IR active modes occurring near 3240, 1505, 1329, and 658 cm^{-1} [114]. These bands are not proof of any coordination since they remain unshifted in the hemin complex. Tests for the presence of these bands should be used solely as a screening technique. The band near 3240 cm^{-1} has been assigned to an N–H stretch of imidazole, proving that the imidazole coordinates through the azanitrogen (–N=) [114].

It is clear that the difference in bound and unbound stretching frequencies may be used as diagnostic tools for some unsaturated small ligands (N_3^-, CN^-, CO, NO, O_2) which have stretching frequencies occurring in a metalloporphyrin window. It is also true that other saturated and/or unsaturated ligands either have no vibrations occurring in the metalloporphyrin window or possess similar bound and unbound spectra, due to size. Such ligands as imidazole, all monatomic ligands (Cl^-, F^-, Br^-, I^-), and saturated small polyatomic molecules (H_2O, NH_3, H_2, etc.) would fall into this category. Unlike imidazole, pyridine does show differences in its bound and unbound spectra [115,131]. For all such molecules, it would become necessary to observe Fe–L_x ($L_x = L_1$ or L_2) stretching frequencies to diagnose their complexation confidently. The five-coordinate M–L stretch spans A_1 and is thus fully allowed in both the Raman and IR, under the veil of C_{4v} symmetry.

Table 8 shows the positions of M–L bands. The Fe(II)–2MeImH Raman stretch for five-coordinate protoporphyrin complexes has been identified near 220 cm^{-1} in water [92]. The hemin Fe–Cl stretch has been identified at 357 cm^{-1} in the IR [114]. The Fe–N_3 stretch occurs near 421 cm^{-1} for Fe(III) octaethyl porphyrin azide [114], while this same stretch occurs near

413 cm^{-1} in metHb–N_3^- (metHb = methemoglobin) [71,114]. The Fe–O_2 stretch has been identified at 567 cm^{-1} in the IR for oxyhemoglobin.

Although Fe(III)–monoimidazole complexes have been identified [114] and isolated [132], no Fe–Im(mono) stretch has ever been reported. The symmetric Fe(III)$(HIm)_2$ porphyrin stretch has been identified at 200 cm^{-1} in the Raman [92]. The asymmetric stretch is located near 377 cm^{-1} in the IR [114]. The symmetric stretch for a Fe(II)–$(pyridine)_2$ species has been identified at 177 cm^{-1} [115], with no report of an asymmetric stretch. Ogoshi [114] has reported Fe–L IR stretching frequencies for a variety of compounds, and many other references are given in Table 8, for both Raman and IR diagnosis. Buchler [131] has also compiled a series of M–L stretching frequencies.

Although oxygen easily binds to heme proteins in a bent "end-on" geometry, the first reported X-ray crystal structure of oxyhemoglobin suggested strain in the heme pocket [133]. The Fe–O–O bond angle was reported as 157°. This angle was much higher than those found in met-hemoglobin cyanide (140°) [134,135], hemoglobin nitrosyl (145°) [115], methemoglobin azide (111–125°) [136,137], or the "picket fence" dioxygen models (133°) [121,138]. The metal is reportedly in or very close to the plane of the porphyrin ring in most low spin hemoglobin complexes (azide [136,137], cyanide [135], carbonyl [139,140], and nitrosyl [115]), and Shannan's structure shows that the metal is no more than 0.016 Å removed from the plane of the porphyrin ring in oxyhemoglobin. Therefore, it appears that most other π-acceptor ligands are forced into sharper angles than oxygen. The iron–oxygen bond distance, 1.6 Å (α chain) [133], is also shorter than those for any hemoglobin system yet studied. These comparisons suggest a better fit in the heme pocket for oxygen than any other ligand. Why oxygen is so special remains a topic of interest, and the exact reasons for its chemistry with hemoglobin are not entirely known.

Like oxygen, the azide ligand binds proteins in a bent end-on arrangement [136,137]. Both have double bonds and lone pairs. Based on the magnitude of the metal–ligand angles, azide fits the heme pocket better than cyanide [135] or carbon monoxide [139], and would seem a likely model for oxygen. Although cyanide, nitrosyl, or carbon dioxide would also serve as approximate models, there are very few or no reports of protoporphyrin-IX carbonyl or nitrosyl complexes. Protoporphyrin-IX cyanide has been prepared in solutions of water [43] and DMSO [36], but is difficult to characterize. None of the above complexes has ever been prepared in the solid state. Of protoporphyrin-IX low spin complexes, only the bis-imidazoles have been characterized by X-ray crystallography [48]. The protoporphyrin-IX azide complex is easily characterized and prepared in solid form as well as in solution. It has been shown to exist in a spin equilibrium in DMSO

[122]. Because of its size and well-behaved chemistry, it is the best nitrogenous ligand for use as an oxygen model.

The vibrational and electronic spectra of oxygen and azide porphyrin complexes shows the oxygen–metal bond to be stronger than the azide–metal bond in hemoglobin. For example, the Fe(II)–O_2 stretch has been identified at 567 cm^{-1} in hemoglobin [102] while the Fe(III)–N_3 stretch has been identified at 421 cm^{-1} in octaethylporphyrin [114] and at 412 cm^{-1} in protoporphyrin-IX azide [123]. It is unlikely that these differences can be solely attributed to a difference in the force constants for Fe–O_2 and Fe–N_3. The atomic weights of azide and oxygen differ by only 10 a.m.u. This difference alone cannot account for the large shifts in the positions of the M–L bands, and other effects (e.g., electronic effects, oxidation state) must be brought to bear to account for this difference. Although a difference in the ring size could cause band positions to shift, the similarity in the position of the Fe–N_3 stretch for met-hemoglobin and protoporphyrin-IX (413 cm^{-1} and 412 cm^{-1}, respectively) suggest that a variation in ring substituents causes little effect. The internal ligand stretches occur at 1156 cm^{-1} and 2060 cm^{-1} for the oxyhemoglobin [141,142] and the protoporphyrin-IX azide complexes [123], respectively. The electronic and vibrational data suggest that the metal–oxygen bond is stronger than the metal–azide bond.

The primary difference between oxygen and azide lies in the fact that oxygen is paramagnetic and exhibits a different π-bonding scheme. Oxygen

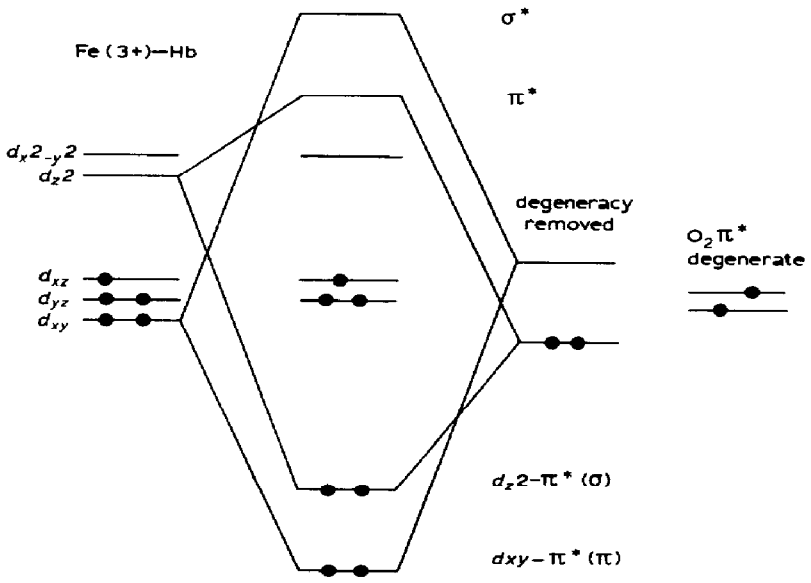

Fig. 12. Molecular orbital energy level diagram for the hypothetical ferric oxyhemoglobin.

donates an electron pair to the metal d_{z^2} σ orbital only after the degeneracy of its π^* orbital has been removed [73]. This degeneracy is removed only when oxygen binds the metal in a bent geometry with the ligand almost parallel to the porphyrin plane. This arrangement optimizes metal–oxygen charge delocalization. In any other arrangement, e.g. perpendicular axial ligation of the oxygen molecule, the π^* orbitals would remain paramagnetic [73]. The paramagnetism would also persist in the high spin ferric state. The molecular orbitals for azide complexes are incapable of such fluxional behavior. The molecular orbital diagrams for met-hemoglobin and oxyhemoglobin are presented in Fig. 12.

(iii) Oxidation state and spin state

The question of how the protein chemistry changes as a function of oxidation state is not easily answered. On the one hand, ligands such as cyanide and imidazole, while preferring the +3 oxidation state, will bind ferrous proteins. Oxygenation of proteins exclusively requires a reduced state for the metal. This is the most difficult obstacle one faces when using ferric model proteins. Since there are no ferric protein models with bound oxygen nor any easily stabilized ferrous oxyproteins, only indirect comparisons can be made.

Although the porphyrin systems compared here are in the ferric state, it is assumed that the ligand also controls the binding site even in the natural ferrous state. While the difference in the oxidation states of the model (+3) and the parent oxygenated protein (+2) are expected to be important for the high spin case ($S = 5/2$), this is not true for the low spin case because the Fe(+3) low spin d^5 orbital arrangement more closely resembles that of a $S = 0$ Fe(+2) arrangement. If the Fe(II)–O_2 bond in hemoglobin is represented by a superoxide formulation [121,137,143], Fe(III)–O_2^-, the differences in oxidated states are further minimized.

A similar Fe(III)–O_2^- charge distribution has been proposed for carbonyl and nitrosyl hemoglobin [146], based on the Mössbauer spectra. These complexes have been widely used as models for oxyhemoglobin. The charge separation for low spin hemoglobin complexes was first theorized by Weiss [147]. Levy and coworkers [145] have shown that deoxy- and met-hemoglobin convert from high to low spin at 210 K. In the deoxy form, the distal histidine wraps around the ring and bonds at the empty axial site. The same behavior is observed for met-hemoglobin once the water ligand is removed. Under these conditions, the comparative effects between the oxidation states of the ferrous protein and a ferric protoporphyrin model are expected to be less significant.

The problems of protein modeling can be represented by protoporphyrin-

IX azide (i.e., using azide to represent oxygen and PPIX to represent hemoglobin). Vibrational information for these two complexes shows that the Fe(II)–O_2 (561 cm^{-1}) bond is stronger than the Fe–N_3 bond of protoporphyrin-IX (412 cm^{-1}). However, the Fe–N_3 stretching frequencies for PPIX-azide and met-hemoglobin azide are nearly equal (412 versus 413 cm^{-1}, respectively). These differences suggest that oxidation state matching is vital for good protein modeling. Further support of this argument is given by the similarity in the Fe–O_2 vibration of oxygenated "picket fence" porphyrins (560 cm^{-1}) and oxyhemoglobin (567 cm^{-1}).

A comparison of M–L stretching frequencies for oxyhemoglobin (567 cm^{-1}) and met-hemoglobin azide (413 cm^{-1}) shows the ferrous complex to have the stronger metal–ligand bond. Oxidation state matching appears to have an effect even for strong π-acid ligands. For example, hemoglobin(+2)NO has an Fe–NO bond length of 1.74 Å [128]. Yet the Fe–CN bond length is 1.98 Å in the Fe(III)–tetraphenylporphyrin cyanide complex [134,135]. Since CN^- and NO are almost equally good π-acceptors, the difference in oxidation states accounts for the large difference in bond order. Nevertheless, this difference in oxidation states is minimized by charge separation between the metal and ligand. There appears to be no compensation for oxidation state differences in high spin complexes, regardless of the nature of the protein or the ligand.

The metal $d\pi \rightarrow$ ligand π^* backbonding increases as the ability of the axial ligand to accept π-density increases. Concurrent with this π-density shift is a decrease in the metal $d\pi \rightarrow$ N(pyr)π^* electron density. This is reflected in the positions of the Fe–N(pyr) frequencies in Fig. 13. The fact that the Fe–L bond involves electron transfer explains why the Fe–O bond of Hb(+2)–O_2 is almost equal to that of Hb(+2)NO. This leads to the conclusion that once oxygen binds the metal in a +2 state, its ability to accept π-density is greatly enhanced over that which it normally exhibits with other non-protein complexes, so much so that it becomes a much better π-acid ligand with native ferro proteins than azide, pyridine, imidazole, cyanide, or even carbon monoxide with ferric proteins. This is a fact which cannot be easily ignored when using model ferric systems.

The merit of ferric models lies in the fact that they are easier to synthesize and easier to characterize. While there is an apparent difference in the chemistry of complexes with differing oxidation states, the fact remains that the models do represent the chemistry of the proteins as faithfully as the ferric state allows.

It has been known for some time that certain vibrations in the 1300–1650 cm^{-1} range are sensitive to structural changes in the hemin core. Properties such as metal spin state ($S = 5/2$, $1/2$, or $3/2$), oxidation state, metal coordination number, N, ($N = 4$, 5 or 6), and ligand π-bonding all have

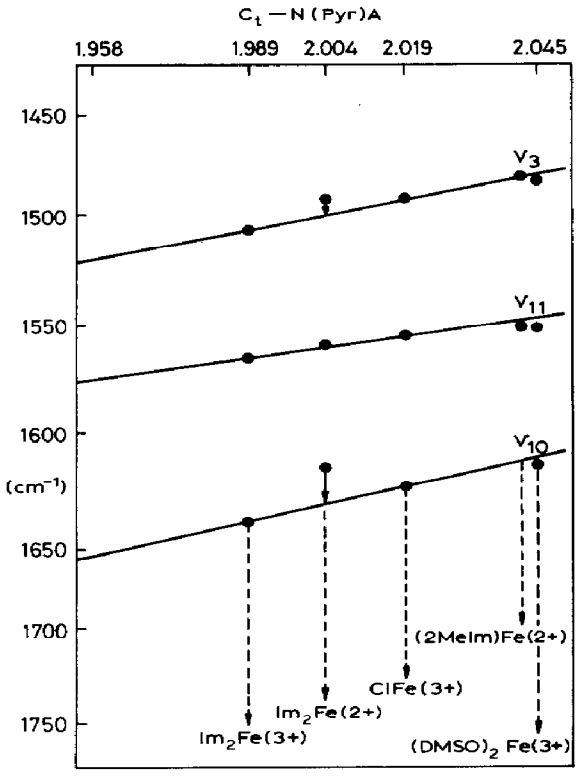

Fig. 13. Porphyrin skeletal mode frequencies versus porphyrin core size. The discrepant frequency points for the ferro complexes are indicated by arrows.

unique frequencies. Spiro and coworkers have identified the Raman stretching frequencies which are most sensitive [88].

Referring to Table 11 and Fig. 10, some trends are immediately obvious. For example, ν_{11}, largely involving double bonded pyrrole carbons, C_b–C_b

TABLE 11

Spin state, oxidation and coordination number marker frequencies

Band	Range	Stretch	Atoms	Sensitive property
I	1350–1375	$4(A_{1g})$	C_a–N(pyr)	Oxidation state
II	1470–1502	$3(A_{1g})$	C_a–C_m	Spin state, π bonding
III	1545–1565	$11(B_{1g})$	C_b–C_b	Spin state, oxidation state, coordination number
IV	1550–1590	$19(A_{2g})$	C_aC_m	Spin state
V	1604–1640	$10(B_{1g})$	C_aC_m	π Bonding, coordination number
	197–234	(A_{1g})	M–N(pyr)	All of the above

Values taken, in part, from ref. 102.

stretching, clearly is dependent on oxidation state of the metal. For six coordinate low spin species, the +3 state shifts ν_{11} to higher frequency than the +2 state (1562 > 1539). Since it is obvious that all high spin species occur at lower frequencies than low spin species for ν_{19} (Band IV), the two bands together tell us both the spin state and oxidation number of the species in question. Band IV may be used to distinguish high spin/low spin species (as could Band II), but not Band III or Band V. Knowing the spin state, Band III and/or Band V would tell us both the oxidation and coordination number.

It is important to point out that no one band is singularly diagnostic of all properties, and all bands should be used to fix the identity of the species. A careful study of Table 11 reveals perceptible trends and easy diagnosis of hemin properties. No such correlations have ever been made for the IR active bands, although the N–H pyrrole stretching frequencies have been correlated with the basicity of the ligand [83]. Since a ligand property is not expected to exert a sizeable perturbation across more than 3 bonds this correlation must be viewed with caution.

Bands V and III are also sensitive to π-backbonding. Spiro [115] has shown that replacement of the poor π-acceptor, imidazole, with a good π-acceptor, cyanide, in Fe(II)–protoporphyrin shifts these bands to higher frequencies. π-backbonding is not expected to be as significant for Fe(III) complexes as for the +2 state analogs, since backbonding is most probable in the Fe(II) oxidation state. If Band III, a C_b–C_b stretch, and Band V, a C_a–C_m stretch, are shifted to higher frequency, this could mean that there is less π-density shifted back into the porphyrin ring and more shifted onto the ligand. For example, cyanide bears a greater measure of electron density than does imidazole. The metal core size is effectively reduced by the electron acceptor properties of the cyanide ion. Oxidation of Fe(II) to Fe(III) lowers the $d\pi$ energy and the effective nuclear charge increases; thus the metal $d\pi \rightarrow$ porphyrin π orbital overlap is less. In the Fe(II) high spin case, the $d\pi$ orbitals are raised in energy, the Fe–N(pyrrole) bond distance is lengthened, and the Fe atom is displaced from the porphyrin plane. All are factors which lessen the overlap of the π-orbitals and diminish the $d\pi \rightarrow$ porphyrin π^* electron interaction. The conditions governing the low spin ferrous states optimize synergic π-effects between the metal and the porphyrin ring.

The M–N(pyrrole) stretch has been correlated with metal core size [90], but this band occurs at very low frequency ($\sim 220\ cm^{-1}$) and resolution in the Raman is difficult because of poor coupling to the $\pi \rightarrow \pi^*$ electronic transition. Nevertheless, it is clear that the metal core size is directly related to all the properties sensitive to Bands I–V. The M–N(pyrrole) distances and the C_t–N(pyrrole) distances have been tabulated, and are shown in

Table 11 and Fig. 13. The C_t–N(pyrrole) distance is the distance from the center of the porphyrin plane to the pyrrole nitrogens. It differs from the M–N(pyrrole) distance only when the Fe atom is not planar.

(iv) Dimerization

UV–visible data may be used to detect dimers. The Soret band near 400 is normally split [57,88] into two bands in aqueous, basic, and alcoholic media, exhibiting 2 UV bands (413, 435 nm) as well as the characteristic 2 bands (α, β) in the visible. The splitting is caused by aggregation resulting from hydrophobic interactions between the porphyrin ring and side chains. The red shift of the Soret band (to longer wavelength) is attributed to exciton splitting [148] and/or stacking interactions [149]. Even though [Fe(III)–PPIX–$(CN)_2$]$^-$ has been shown to be stacked, exciton splitting does not depend on stacking and since the aggregating process is known to be time dependent (occurring over a period of hours or days) purely lateral interactions could account for the dimerizations [149]. The Q band (α and β bands) are not generally split in low spin complexes which exhibit dimerization. Charge transfer bands in some dimerized high spin hemins may disappear to form one broad unresolved band in the visible region [41].

IR spectra of hemin dimers are more difficult. Deuterohemin exhibits an Fe–O–Fe asymmetric stretch near 840 cm^{-1} in KBr pellets [41]. Some other stretches are represented by Fe=O (820–1100 cm^{-1}), Fe–O (450–650 cm^{-1}), FeO–H ($\sim$ 3580–3640 cm^{-1}), and Fe–O–Fe (630–900 cm^{-1}) [41,131]. Dimerization reactions of hemins with aqueous ligand solution are extremely involved and may be present as a singularly bridged O, a doubly bridged hydroxo, a mixed doubly bridged hydroxo/ligand complex, and many other forms. Dimerization reactions have been studied diligently by many [41,131,150–152] and detailed information should be sought in the references cited.

ACKNOWLEDGEMENT

C.J.O. thanks the Edward G. Schlieder Educational Foundation for support during the preparation of this manuscript.

REFERENCES

1 (a) J.P. Collman, Acc. Chem. Res., 10 (1977) 265.
(b) J.A. Ibers and R.H. Holm, Science, 204 (1980) 233.
2 T. Hashimoto, R.L. Dyer, M.J. Crossley, J.E. Baldwin and F. Basolo, J. Am. Chem. Soc., 104 (1982) 2101.
3 D.M. Collins, R. Countryman and J.L. Hoard, J. Am. Chem. Soc., 94 (1972) 2066.

4 L.J. Radonovich, A. Bloom and J.L. Hoard, J. Am. Chem. Soc., 94 (1972) 2073.
5 W.R. Scheidt, I.A. Cohen and M.E. Kassner, Biochemistry, 18 (1979) 3546.
6 P.K. Warme and L.P. Hager, Biochemistry, 9 (1970) 1606.
7 D.H. Dolphin, J.R. Sams and T.B. Tsin, Inorg. Chem., 16 (1977) 711.
8 J. Fuhrhop and K.M. Smith in K. Smith (Ed.), Porphyrins and Metalloporphyrins, Elsevier, Amsterdam, 1975, pp. 808–811.
9 H. Fisher, Org. Synth., 3 (1955) 442.
10 (a) T.C. Chu and E.J. Chu, J. Biol. Chem., 212 (1955) 1.
(b) R.F. Labbe and G. Nishida, Biochim. Biophys. Acta., 26 (1957) 437.
11 (a) R. Lemberg and J. Barrett, Cytochromes, Academic Press, London, 1973.
(b) E.M. Colleran and O.T.G. Jones, Biochem. J., 134 (1973) 89.
12 L. Pauling, The Nature of the Chemical Bond, 3rd. edn., Cornell University Press, Ithaca, New York, 1960.
13 M.F. Perutz, J. Cryst. Growth, 2 (1968) 54.
14 M.F. Perutz, Nature (London), 228 (1970) 726.
15 M.F. Perutz, Nature (London), 237 (1972) 495.
16 M.F. Perutz and C.F. Ten Eyck, Cold Springs Harbor Symp., Quant. Biol., 36 (1971) 315.
17 F. Basolo, B.M. Hoffman and J.A. Ibers, Acc. Chem. Res., 8 (1975) 384.
18 B. Shannon, J. Mol. Biol., 171 (1983) 31.
19 J.M. Baldwin, J. Mol. Biol., 136 (1980) 103.
20 H.A. Harbury and P.A. Loach, J. Biol. Chem., 235 (1960) 12.
21 R.J. Kassner and D.C. Blumenthal, J. Biol. Chem., 255 (1980) 12, 5859.
22 R.J. Kassner and Y.J. Huang, J. Biol. Chem., 256 (1981) 11, 5327.
23 R.J. Kassner and D.C. Blumenthal, J. Biol. Chem., 254 (1979) 9617.
24 R.J. Kassner and Y. Huang, J. Am. Chem. Soc., 101 (1979) 19, 5807.
25 R.J. Kassner and Y. Huang, J. Am. Chem. Soc., 103 (1981) 4927.
26 G. McLendon and M. Smith, Inorg. Chem., 21 (1982) 847.
27 G. McLendon and M. Smith, J. Am. Chem. Soc., 103 (1981) 4912.
28 G. McLendon and M. Smith, J. Am. Chem. Soc., 102 (1980) 5666.
29 J.W. Buchler, in K. Smith (Ed.), Porphyrins and Metalloporphyrins, Elsevier, Amsterdam, 1975, pp. 157–163.
30 K. Smith, in K. Smith (Ed.), Porphyrins and Metalloporphyrins, Elsevier, Amsterdam, 1975, pp. 11–15.
31 D.F. Koenig, Acta Crystallogr., 18 (1965) 663.
32 J. Shack and W.M. Clark, J. Biol. Chem., 171 (1947) 143.
33 K. Kaziro, F. Uchimura and G. Kikuchi, J. Biochem. (Tokyo), 43 (1956) 539.
34 G.N. Lamar, J. Del Gaudio and J.S. Frye, Biochim. Biophys. Acta., 498 (1977) 422.
35 E. Antonini and M. Brunori, Hemoglobin and Myoglobin in their Reactions with Ligands, North-Holland, Amsterdam, 1971.
36 G.N. LaMar and V.P. Chacko, J. Am. Chem. Soc., 104 (1982) 7002.
37 F. Ann Walker, Man-Wai Lo and M.T. Ree, J. Am. Chem. Soc., 98 (1976) 5552.
38 H.A.O. Hill and K.G. Morallee, J. Chem. Soc. D, (1970) 266.
39 P.L. Richards, W.S. Caughey, H. Eberspaecher, G. Fehrer and M. Malley, J. Chem. Phys., 47 (1967) 1187.
40 W.R. Scheidt and M. Gouterman, in H. Gray and A.B.P. Lever (Eds.), Iron Porphyrins Part 1, Elsevier, New York, 1983, p. 101.
41 W.S. Caughey, W.H. Fuchsman, H.I. Eberspaecher and N. Sadasivian, Biochemistry, 8 (1969) 534.

42 (a) J.O. Alben, W.H. Fuchsman, C.A. Beaudreaux and W.S. Caughey, Biochemistry, 7 (1968) 624.
(b) J.C. Maxwell and W.S. Caughey, Biochemistry, 15 (1976) 388.
43 W.S. Caughey and S. McCoy, Biochemistry, 9 (1970) 2387.
44 R.J.P. Williams and D.W. Smith, Struct. Bonding (Berlin), 7 (1970) 1.
45 C.A. Reed, T. Mashiko, S.P. Bentley, M.E. Kastner, W.R. Scheidt, K. Spartalian and G. Lang, J. Am. Chem. Soc., 101 (1979) 2948.
46 C.C. Jorgensen, Oxidation Number and Oxidation States, Springer, New York, 1969, p. 84.
47 H. Huheey, Inorganic Chemistry, 3rd edn., Harper and Row, Cambridge, 1983.
48 R.G. Little, K.R. Dymock and J.A. Ibers, J. Am. Chem. Soc., 97 (1975) 4532.
49 J.W. Buchler, in D. Dolphin (Ed.), The Porphyrins, Vol. 1, Part A, Academic Press, New York, 1978, p. 389.
50 E.B. Fleischer, S. Jacobs and L. Mestichelli, J. Am. Chem. Soc., 90 (1968) 2527.
51 J.W. Buchler, in D. Dolphin (Ed.), The Porphyrins, Vol. 1, Part A, Academic Press, New York, 1978, p. 389; K.F. Purcell and J.C. Kotz, ibid., chap. 13, p. 704.
52 W.R. Scheidt, K.J. Haller and K. Hatano, J. Am. Chem. Soc., 102 (1980) 3017.
53 W.R. Scheidt, K.J. Haller, Y.J. Lee, W. Luangdilok, K. Anzai and K. Hatano, Inorg. Chem., 22 (1983) 1516.
54 K.M. Kadish, in H. Gray and A.B.P. Lever (Eds.), Iron Porphyrins Part 1, Elsevier, New York, 1983, pp. 161–245.
55 (a) K.M. Kadish and D.G. Davis, Ann. N.Y. Acad. Sci., 206 (1973) 495.
(b) K.M. Kadish, M.M. Morrison, L.A. Constant, D.G. Davis and L. Dickens, J. Am. Chem. Soc., 98 (1976) 8387.
56 G.N. Lamar and M. Zobrist, J. Am. Chem. Soc., 100 (1978) 1944.
57 L.J. Boucher, J. Am. Chem. Soc., 90 (1968) 6640.
58 M. Momentum, J. Mispelter and D. Lexa, Biochim. Biophys. Acta, 320 (1973) 652.
59 W.R. Scheidt, Y.J. Lee, S. Tamai and K. Hatano, J. Am. Chem. Soc., 105 (1983) 778.
60 R.G. Pearson, J. Am. Chem. Soc., 85 (1963) 3533.
61 R.G. Pearson, J. Chem. Educ., 45 (1968) 581.
62 R.G. Pearson, J. Chem. Educ., 45 (1968) 643.
63 J.L. Hoard, Ann. N.Y. Acad. Sci., 206 (1973) 18.
64 J.L. Hoard, D.M. Collins and W.R. Schoidt, J. Am. Chem. Soc., 94 (1972) 6689.
65 T. Mashiko, M.E. Kastner, K. Spartalian, W.R. Scheidt and C.A. Reed, J. Am. Chem. Soc., 100 (1978) 6354.
66 T.G. Spiro, J.D. Stong and P. Stein, J. Am. Chem. Soc., 101 (1979) 2648.
67 S.E.V. Phillips, J. Mol. Biol., 142 (1980) 531.
68 R.J.P. Williams and D.W. Smith, Struct. Bonding (Berlin), 7 (1970) 1.
69 A.S. Brill and R.J.P. Williams, Biochem. J., 78 (1961) 246.
70 H. Kobayashi, Y. Yanagawa, H. Osada, S. Minami and M. Shimizu, Bull. Chem. Soc. Jpn., 46 (1973) 1471.
71 W.S. Caughey, in I. Eichhorn (Ed.), Inorganic Biochemistry, Vol. 2, Elsevier, Amsterdam, 1973, p. 797.
72 M. Gouterman, in D. Dolphin (Ed.), The Porphyrins, Vol. 3, Academic Press, New York, 1978, Chap. 1.
73 M. Zerner, M. Gouterman and H. Kobayashi, Theor. Chim. Acta (Berlin), 6 (1966) 363.
74 M. Gouterman, Ann. N.Y. Acad. Sci., 206 (1973) 70.
75 M.W. Makinen and W.A. Eaton, Ann. N.Y. Acad. Sci., 206 (1973) 210.
76 M.W. Makinen and A.K. Churg, in H.B. Gray and A.B.P. Lever (Eds.), Iron Porphyrins, Part 1, Elsevier, New York, 1983, p. 101.

77 D.A. Sweigart and M.M. Doeff, Inorg. Chem., 21 (1982) 3699.
78 S.B. Brown and I.R. Lantzke, J. Biochem., 115 (1969) 279.
79 W.A. Eaton and E.J. Charney, Chem. Phys., 51 (1969) 4502.
80 W.A. Eaton and E.J. Charney, in B. Chance, C.P. Lee and J.K. Blaise (Eds.), Probes of Structure and Function of Macromolecules and Membranes, Vol. I, Academic Press, New York, 1971, pp. 155–164.
81 D. Kellin and E.F. Hartree, Biochem. J., 49 (1951) 88.
82 A.D. McLauren and D. Shugar, in Photochemistry of Proteins and Nucleic Acids, Pergamon, The Macmillan Co., New York, 1964, p. 110.
83 J.O. Alben, S.S. Choi, A.D. Alder and W.S. Caughey, Ann. N.Y. Acad. Sci., 206 (1973) 278–295.
84 Thomas G. Spiro in A.P.B. Lever and Harry Gray (Eds.), Iron Porphyrins, Part 2, Elsevier, New York, 1983, pp. 89–159.
85 Hans Burger in K.M. Smith (Ed.), Porphyrins and Metalloporphyrins, Elsevier, New York, 1975, pp. 525–534.
86 T.G. Spiro, K.C. Langry, S. Choi and K.M. Smith, J. Am. Chem. Soc., 104 (1982) 4337–4344.
87 T.G. Spiro, S. Choi, J.J. Lee and Y.H. Wei, J. Am. Chem. Soc., 105 (1983) 3692–3707.
88 T.G. Spiro and S. Choi, J. Am. Chem. Soc., 105 (1983) 3683–3692.
89 G.T. Babcock and P.M. Callahan, Biochemistry, 20 (1981) 952–958.
90 T.G. Spiro, K.C. Langry, K.M. Smith, D.L. Budd and G.N. LaMar, J. Am. Chem. Soc., 104 (1982) 4345–4351.
91 G. Sievers, K. Osterlund and N. Ellfolk, Biochim. Biophys. Acta, 581 (1979) 1–14.
92 A. Desbois and M. Lutz, Biochim. Biophys. Acta, 671 (1981) 168, 257.
93 L.D. Spandling, C.C. Chang, Nai-Teng Yu and R.H. Felton, J. Am. Chem. Soc., 97 (1975) 2517–2525.
94 B.N. Figgis, Introduction to Ligand Field Theory, Interscience, New York, 1966.
95 W.M. McClain, J. Chem. Phys., 55 (1971) 2789.
96 T.G. Spiro and T.C. Strekas, J. Am. Chem. Soc., 96 (1974) 338.
97 F.A. Cotton, Chemical Applications of Group Theory, 2nd. edn., Wiley-Interscience, New York, 1971.
98 R.S. Drago, Physical Methods in Inorganic Chemistry, W.B. Saunders, Philadelphia, 1977.
99 J.H. Hibben, The Raman Effect and its Chemical Applications, Reinhold, New York, 1939.
100 M. Abe, T. Kitagawa and Y. Kyogoku, J. Chem. Phys., 69 (1978) 4526–4534.
101 C.M. Wang and W.S. Brinigar, Biochemistry, 18 (1979) 4960–4977.
102 H. Brunner, Naturwissenschaften, 61 (1974) 129.
103 J.M. Burke, J.R. Kincaid, S. Peters, R.R. Gagne, J.P. Collman and T.G. Spiro, J. Am. Chem. Soc., 100 (1978) 6083.
104 M.A. Walters, T.G. Spiro, K.S. Suslick and J.P. Collman, J. Am. Chem. Soc., 102 (1980) 6857.
105 H. Hori and T. Kitagawa, J. Am. Chem. Soc., 102 (1980) 3608.
106 M. Tsubaki, K. Nagai and T. Kitagawa, Biochemistry, 19 (1980) 379.
107 J.D. Stong, J.M. Burke, P. Daly, P. Wright and T.G. Spiro, J. Am. Chem. Soc., 102 (1980) 5815.
108 M. Tsubaki, R.B. Srivastava and N.T. Yu, Biochemistry, 21 (1982) 1132.
109 M.A. Walters, T.G. Spiro and J.P. Collman, Biochemistry, 21 (1982) 6989.
110 S.A. Asher, L.E. Vickery, T.M. Schuster and K. Sauer, Biochemistry, 16 (1977) 5849.

111 M. Tsubaki, R.B. Srivastava and N.T. Yu, Biochemistry, 20 (1981) 946.
112 J. Teraoka and T. Kitagawa, J. Biol. Chem., 96 (1981) 3969.
113 P.M. Champion, B.R. Stallard, G.C. Wagner and I.C. Gunsalus, Dev. Biochem., 23 (1982) 547.
114 H. Ogoshi, E. Watanabe, Z. Yoshida, J. Kincaid and K. Nakamoto, J. Am. Chem. Soc., 95 (1973) 2845–2849.
115 T.G. Spiro and M. Burke, J. Am. Chem. Soc., 98 (1976) 5487.
116 J.P. Collman, J.L. Hoard, N. Kim, G. Land and C.A. Reed, J. Am. Chem. Soc., 97 (1975) 2676.
117 M.E. Kastner, W.R. Scheidt, T. Mashiko and C.A. Reed, J. Am. Chem. Soc., 100 (1978) 666.
118 T. Mashiko, C.A. Reed, K.J. Haller, M.E. Kastner and W.R. Scheidt, J. Am. Chem. Soc., 103 (1981) 5757.
119 J.L. Hoard, G.H. Cohen and M.D. Glick, J. Am. Chem. Soc., 89 (1967) 1992.
120 J.L. Hoard and W.R. Scheidt, Proc. Natl. Acad. Sci., U.S.A., 70 (1973) 3919.
121 W.T. Robinson, G.B. Jameson, G.A. Rodley, R.R. Gagne, C.A. Reed and J.P. Collman, Inorg. Chem., 17 (1978) 850–857.
122 I. Morishima and S. Neya, J. Am. Chem. Soc., 104 (1982) 5658–5661.
123 J.W. Owens, Ph.D. Thesis, University of New Orleans, 1986.
124 W.S. Caughey, C.H. Barlow, D.H. O'Keefe and M.C. O'Toole, Ann. N.Y. Acad. Sci., 206 (1973) 296.
125 L. Vaska, Acc. Chem. Res., 9 (1976) 175.
126 J.F. Deathridge, J. Mol. Biol., 134 (1979) 419.
127 J.B. Dunn, D.F. Shriver and I.M. Klotz, Proc. Natl. Acad. Sci., U.S.A. 70 (1973) 2582.
128 J.F. Deathridge and K. Moffat, J. Mol. Biol., 134 (1979) 401.
129 J.A. Ibers, F.S. Molinero, G. Jameson, J.P. Collman, J.I. Brauman, E. Rose and K.S. Suslick, J. Am. Chem. Soc., 100 (1978) 6769.
130 F. Basolo, B.M. Hoffman and J.A. Ibers, Acc. Chem. Res., 8 (1975) 384.
131 J.W. Buchler in D. Dolphin (Ed.), The Porphyrins, Vol. 1, Part A, Academic Press, New York, 1978, p. 420.
132 L. Bullard, R.M. Panaya, A.N. Thorpe and P. Hambright, Bioinorg. Chem., 3 (1974) 161–164.
133 B. Shaanan, J. Mol. Biol., 171 (1983) 31.
134 W. Steigman and E. Weber, J. Mol. Biol., 127 (1979) 309.
135 J.F. Deathridge, R.S. Loe, C.M. Anderson and K. Moffat, J. Mol. Biol., 104 (1976) 687.
136 L. Stryer, J.C. Kendrew and H.C. Watson, J. Mol. Biol. 8 (1964) 96.
137 J.F. Deathridge, S.K. Obendorf and K. Moffat, J. Mol. Biol. 134 (1979) 419.
138 (a) W.T. Robinson, G.B. Jameson, J.P. Collman and T.N. Sorrell, Inorg. Chem. 17 (1978) 858–863.
(b) J.A. Ibers, F.S. Molinaro, G.B. Jameson, J.P. Collman, J.I. Brauman, E. Rose and K.S. Suslick, J. Am. Chem. Soc., 100 (1978) 6769.
139 E.J. Heidner, R.C. Ladner and M.F. Perutz, J. Mol. Biol., 104 (1976) 707.
140 J.M. Baldwin, J. Mol. Biol., 136 (1980) 103.
141 J.O. Alben, G.H. Bare and P.P. Moh, in W.S. Caughey (Ed.), Biochemical and Clinical Aspects of Hemoglobin in Abnormalities, Academic Press, New York, 1978, p. 607.
142 M. Tsubaki and N.T. Yu, Proc. Natl. Acad. Sci. U.S.A., 78 (1981) 3581.
143 J.P. Collman, Proc. Natl. Sci., U.S.A., 73 (1976) 3333.
144 M. Cerdonio, A. Congio-Costellano, F. Mogno, C. Pispisa, G.L. Romain and S. Vitale, Proc. Natl. Acad. Sci. U.S.A., 74 (1977) 398.

145 A. Levy and J.M. Rifkin, Biochemistry, 24 (1985) 6050.
146 G. Lang and W. Marshall, Proc. Phys. Soc., 87 (1966) 3.
147 J.J. Weiss, Nature (London), 202 (1964) 83.
148 R. Selencky, D. Holten, M.W. Windsor, J.B. Paine, D. Dolphin, M. Gouterman and J.C. Thomas, Chem. Phys., 60 (1981) 33–46.
149 G.N. Lamar and D.B. Viscio, J. Am. Chem. Soc., 96 (1974) 7354–7355.
150 G.N. Lamar, Der-Hang Chin and A.L. Balch, J. Am. Chem. Soc., 102 (1980) 4344–4349.
151 K.M. Kadish, L.A. Bottomley, J.G. Brace and N. Winogard, J. Am. Chem. Soc., 102 (1980) 4341–4344.
152 P. Hambright, Porphyrins and Metalloporphyrins, Elsevier, New York, 1975, p. 268.
153 W.A. Eaton, L.K. Hanson, P.J. Stephens, J.C. Sutherland and J.B.R. Dunn, J. Am. Chem. Soc., 100 (1978) 4991.
154 W.A. Eaton and R.M. Hochstrasser, J. Chem. Phys., 49 (1968) 985.
155 M.W. Makinen, A.K. Churg and H.A. Glick, Proc. Natl. Acad. Sci. U.S.A., 75 (1978) 2291.
156 A.K. Churg and M.W. Makinen, J. Chem. Phys., 68 (1978) 1913.
157 J.S. Philo, U. Dreyer and T.M. Schuster, Biochemistry, 23 (1984) 865.
158 C.J. O'Connor, C.J. Hamilton and J.W. Owens, Inorg. Chim. Acta, 93 (1984) 55.